

DOKUZ EYLÜL UNIVERSITY
GRADUATE SCHOOL OF NATURAL AND APPLIED
SCIENCES

3D MOTION TRACKING AND ANALYSIS OF
MICROORGANISMS FOR ECOTOXICITY
TESTING

by
Ali Emre KAVUR

July, 2014
İZMİR

3D MOTION TRACKING AND ANALYSIS OF MICROORGANISMS FOR ECOTOXICITY TESTING

**A Thesis Submitted to the
Graduate School of Natural And Applied Sciences of Dokuz Eylül University
In Partial Fulfillment of the Requirements for the Degree of Master of Science in
Electronics Engineering**

**by
Ali Emre KAVUR**

**July, 2014
İZMİR**

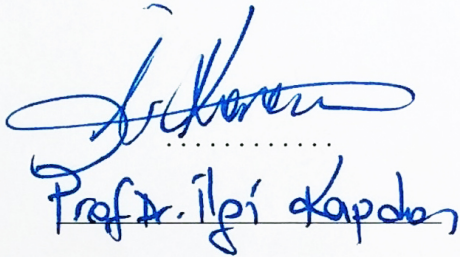
M.Sc THESIS EXAMINATION RESULT FORM

We have read the thesis entitled "**3D MOTION TRACKING AND ANALYSIS OF MICROORGANISMS FOR ECOTOXICITY TESTING**" completed by **ALİ EMRE KAVUR** under supervision of **ASST. PROF. DR. GÜLESER KALAYCI DEMİR** and we certify that in our opinion it is fully adequate, in scope and in quality, as a thesis for the degree of Master of Science.

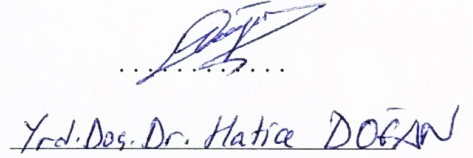


Asst. Prof. Dr. Güleser KALAYCI DEMİR

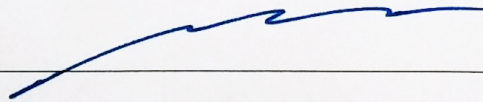
Supervisor



Jury Member



Jury Member



Prof. Dr. Ayşe OKUR

Director

Graduate School of Natural and Applied Sciences

ACKNOWLEDGEMENTS

I would like to offer my special thanks to my supervisor Asst.Prof. Dr. Güleser KALAYCI DEMİR, for the valuable guidance and support during the planning and development of this research project.

Support given by Dr. Levent ÇAVAŞ has been of great help in planing chemical experimental works in this project.

I would like to thank to my colleague and friend Gökhan TIĞLISEL for helping in purchasing hardware and contributions to design of the vision system.

I would like also to thank to Asst.Prof. Dr. Mustafa Alper SELVER for supporting me during my graduate education.

Last but not least, I wish to thank my parents and friends for their support and encouragement throughout my study.

This thesis was supported by 2012.KB.FEN.073 DEU-BAP project.

Ali Emre KAVUR

3D MOTION TRACKING AND ANALYSIS OF MICROORGANISMS FOR ECOTOXICITY TESTING

ABSTRACT

Motility of test microorganisms is an essential focus of ecotoxicity testing. Since broad diversity of motion behaviour causes misinterpolation and limits test analysis, objective and quantitative methods should be used to analyse microorganisms motility. In this thesis, a new vision-based computational method based on the movement characteristics is proposed to analyse the effect of the toxic material on the organism.

Motions of *Artemia salina*, a widely used test microorganism in ecotoxicity testing, were captured by an implemented 3D vision system set-up. The system contains two industrial GigE Vision cameras. A Stereo Vision capture software was developed under Microsoft Visual C# Express with the help of SDK library provided by The Imaging Source GmbH company.

Artemia salina at instar II-III naupilar stages were observed by three minutes recordings with one hour interval under different amounts of *potassium dichromate* (a kind of toxic chemical) included water until death of *Artemia salina*. After recording process, 3D centroid position of each *Artemia salina* was determined and motion path related features such as linearity, wobble and fractal dimensions were obtained. These features were used to classify the motion behaviour of *Artemia salina* into four different classes, namely; straight, curly, semi-complex, complex. The classification was performed by using an artificial neural network. Results shows that motion behaviours were classified with high accuracy and can be used effectively for ecotoxicity testing purposes.

Keywords: 3D motion, stereo vision, motion analysis, *Artemia salina*, toxicity testing

EKOTOKSİK LİK TESTLERİ İÇİN MİKROORGANİZMALARIN 3B HAREKET İZLEMESİ VE ANALİZİ

ÖZ

Test mikroorganizmaların hareketi ekotoksikoloji testlerinin gerçekleştirilmesi için gerekli bir özelliktir. Çevredeki toksik maddeler canlıların davranışlarında değişikliğe neden olur. Canlının çok çeşitli davranış şekillerinin olması yanlış değerlendirmeye ve analizleri sınırlandırmaya sebep olduğu için objektif ve niceliksel metotlar analiz için kullanılmalıdır. Bu tezde, hareket karakteristiğine bağlı olan yeni görüntüleme temelli bir hesaplama yöntemi, toksik maddelerin organizmanın hareket davranışları üzerinde etkisini analiz etmek için sunulmaktadır.

Ekotoksisite testlerinde sık olarak kullanılan *Artemia salina*'nın hareketleri, 3B görüntüleme uygulamalı bir sistem düzeneği ile kayıt edilmiştir. Bu sistem iki endüstriyel GigE Vision kamera içermektedir. Bir adet stereo görüntü kayıt yazılımı Microsoft Visual C# Express ortamında, The Imaging Source GmbH firmasının sağladığı SDK kütüphanesi yardımı ile geliştirilmiştir.

Instar II-III evresindeki *Artemia salina*'lar ölene kadar birer saatlik aralıklarda üç dakika boyunca değişik miktarlarda *potasyum dikromat* (bir çeşit toksik madde) içeren sularda gözlemlenmiştir. Kayıt işleminden sonra *Artemia salina*'ların 3B merkezi koordinatları tespit edilmiş ve hareket şekilleri ile ilgili linearity, wobble, fractal dimensions gibi öznitelikleri elde edilmiştir. Bu öznitelikler *Artemia salina*'nın hareket karakteristiğini straight, curly, semi-complex, complex isimli dört farklı gruba ayırmak için kullanılmıştır. Sınıflandırma işlemi yapay sinir ağları ile gerçekleştirilmiştir. Sonuçlar hareket davranışlarının yüksek performans ile sınıflandırıldığını ve efektif şekilde ekotoksisite testinde kullanılabileceğini göstermiştir.

Anahtar kelimeler: 3B hareket, stereo vision, hareket analizi, *Artemia salina*, toksisite testi

CONTENTS

	Page
THESIS EXAMINATION RESULT FORM.....	ii
ACKNOWLEDGEMENTS	iii
ABSTRACT	iv
ÖZ	v
LIST OF FIGURES	ix
LIST OF TABLES	x
CHAPTER ONE – INTRODUCTION	1
1.1 3D Motion Tracking Techniques	3
1.2 Stages of the Project	6
CHAPTER TWO – HATCHING THE TEST ORGANISM AND PREPARING THE TOXIC MATTER	7
CHAPTER THREE – 3D VIDEO CAPTURE SYSTEM.....	10
3.1 Capture System Hardware.....	10
3.1.1 Hardware Set-up	10
3.1.2 Camera.....	12
3.1.3 Lens.....	15
3.2 Calibration of Set-up.....	16
3.3 Video Capture System Software	17
CHAPTER FOUR – OBJECT DETECTION AND TRACKING	21
CHAPTER FIVE – MOTION ANALYSIS AND CLASSIFICATION	25
5.1 Motion Feature Extraction	25
5.2 Motion Classification	29

5.2.1 Motion Classes	29
5.2.2 Classification Method	31
5.2.3 Classification Results	34
 CHAPTER SIX – RESULTS OF ECOTOXICITY ANALYSIS AND MOTION BEHAVIOR CLASSES.....	 37
 CHAPTER SEVEN – CONCLUSION	 42
 REFERENCES.....	 44

LIST OF FIGURES

	Page
Figure 1.1 Digital holographic microscopy	3
Figure 1.2 Micropillar based PDMS device inside	4
Figure 1.3 Micropillar based PDMS device on work	4
Figure 1.4 Working principle of Hawk-Eye system football	5
Figure 1.5 Sections of the systems	6
Figure 2.1 Life cycle of Artemia Salina	7
Figure 2.2 Hatching of Artemia Salina	7
Figure 2.3 Naupliar stages of Artemia Salina.....	8
Figure 2.4 Hatching tube.....	9
Figure 3.1 System set-up.....	10
Figure 3.2 System set-up picture	11
Figure 3.3 Observation cuvette.....	11
Figure 3.4 Static IP configuration of cameras.....	13
Figure 3.5 I/O ports of DFK 23G618.....	14
Figure 3.6 Diagram of trigger circuit.	14
Figure 3.7 Timing diagram of DFK 23G618	15
Figure 3.8 Picture of Tamron M118FM25	16
Figure 3.9 Calibration of system.....	17
Figure 3.10 Stereo Recorder Software	18
Figure 3.11 Camera settings sections	18
Figure 3.12 Recording settings window	19
Figure 4.1 Approximate median results	22
Figure 4.2 Motion samples of Artemia nauplius	23
Figure 4.3 Results of smoothing on motion paths.	24
Figure 5.1 Calculation of V_C , V_A , V_S	26
Figure 5.2 Different L and W combinations samples	27
Figure 5.3 Distribution example of V_C , V_A , V_S according to motion types.	28

Figure 5.4	Straight motion sample	29
Figure 5.5	Curly motion sample	30
Figure 5.6	Semi-complex motion sample	30
Figure 5.7	Complex motion sample.....	31
Figure 5.8	Plot of L , W and Df	32
Figure 5.9	Diagram of artificial neural network.....	32
Figure 5.10	Relations between motion types and features	36
Figure 6.1	<i>Artemia</i> nauplii in control group.....	37
Figure 6.2	<i>Artemia</i> nauplii in 100 mg/L $K_2Cr_2O_7$	38
Figure 6.3	<i>Artemia</i> nauplii in 125 mg/L $K_2Cr_2O_7$	38
Figure 6.4	<i>Artemia</i> nauplii in 150 mg/L $K_2Cr_2O_7$	38
Figure 6.5	<i>Artemia</i> nauplii in 175 mg/L $K_2Cr_2O_7$	39
Figure 6.6	<i>Artemia</i> nauplii in 200 mg/L $K_2Cr_2O_7$	39
Figure 6.7	Time and toxic matter plot.....	39
Figure 6.8	Timeline chart of an <i>Artemia</i> nauplius sample.....	40

LIST OF TABLES

	Page
Table 3.1 Specifications of DFK 23G618.....	13
Table 3.2 Specifications of M118FM25	16
Table 5.1 Confusion matrix of network with all features.....	34
Table 5.2 Confusion matrix of network without sub-features.....	35
Table 6.1 All results of control trials	40
Table 6.2 All results of toxic included trials	41

CHAPTER ONE

INTRODUCTION

Motion analysis of an organism, a cell or an animal is a popular research area in literature for different purposes such as cellular differentiation (Ghanbari et al., 2012), fertility (Jasko, 1990) and application to robotics (Sudo et al., 2008). Motions mechanism of organisms in nature may help to handle a problem or to gain an ability to artificial systems. This fact makes motion analysis of organisms very popular for toxicity testing (Svensson & Mathiasson, 2005; Alyuruk et al., 2013; Kokkali et al., 2011).

Toxicity testing has an important role in many areas such as biochemical analysis, food production and chemical industry (James et al., 2003). Beyond this, conducting toxicology testing might also be beneficiary for environmental and safety investigations in order to detect harmful material and keep environmental balance.

There are several methods for toxicity testing, however these methods need advanced and rarely found systems. On the other hand, bioassay is an alternative method for handling this problem. Bioassay involves the use of a live animal to determine the biological activity of a substance. Bioassay depends to measure the effects of a substance on a living organism. It is a helpful method in the development of new drugs and in monitoring environmental pollutants. In order to detect the toxicity level of a substance, a chosen model organism should be incubated in a solution containing the substance. After a certain time period, the number of the organisms showing a pre-defined effect is used to define toxicity level. Some organisms as *Vibrio fischeri* and *Artemia salina* are used for applications of bioassay (Panagoula et al., 2002; Hernando et al., 2003).

Artemia salina is a kind of brine shrimp that lives in saline water - in salty lakes commonly (Britannica, 2014). Their food sources are microorganisms living in that water. *Artemia salina* is widely used commercial fish food in aquariums. Production method of them is hatching from dried cysts. Following the hatching, the size of *Artemia* larvae are about 1-2 mm while adult ones can grow up to 15 mm. Besides

being aquarium fish feed, *Artemia salina* is used for toxicity testing of chemicals. (Svensson & Mathiasson, 2005) *Artemia* is resistant against some toxic chemicals species. Besides, it can adapt to many varied environmental conditions (Koutsaftis & Aoyama, 2007; Barahona & Sánchez-Fortún, 1999). Due to its living conditions, it has ability to tolerate high amount of salt concentrations. Moreover, it is easy to culture, widely available on market and has short generation time with potential economical benefit (Panagoula et al., 2002; Okamura, 2000; Koutsaftis & Aoyama, 2008; Bartolomé & Sánchez-Fortún, 2005; Koutsaftis & Aoyama, 2007). These advantages make it a popular research organism for toxicity testing (Ruebhart et al., 2008).

Many bioassay applications are performed by human observation. However, this is not an efficient method while working with organisms which have fast and discontinuous moving. To overcome this problem, automatic or semi-automatic video tracking systems have been proposed (Alyuruk et al., 2013; Kokkali et al., 2011). The main advantage of these systems is being able to catch and track fast movements and enabling quantitative analysis. Human eye cannot distinguish motions faster than 30 fps. On the other hand, a digital camera can capture more than 30 fps depending on its specifications. Another advantage of the video tracking is focusing on small objects. It is impossible to see tiny organisms by human eye. Also some barely seen organisms' motion cannot be tracked continuously. Because of this problems, many organisms are collected in same medium and they are observed together in human based applications. Nevertheless, a digital video tracking system is able to zoom and focus on only one or a small group of organism. This competency of the system provides precise and detailed information about the motion behavior of targeted organisms. Movements of creatures are three dimensional in the nature so 3D motion tracking has many advantages than 2D applications. The main benefit is the ability to obtain detailed and precise results that can be used for quantitative analysis and modelling.

1.1 3D Motion Tracking Techniques

There are different approaches for 3D motion tracking in literature. For example, digital holographic microscopy is a precise method that is used for some researches and applications (Lee & Seo, 2011; Sheng et al., 2006; Choi & Lee, 2009). Digital holographic microscopy does not record captured image directly, it records the light wave front derived from object (Figure 1.1). The reference light and object's light interfered by beam splitter. The result light which is called hologram is captured by CCD sensor.

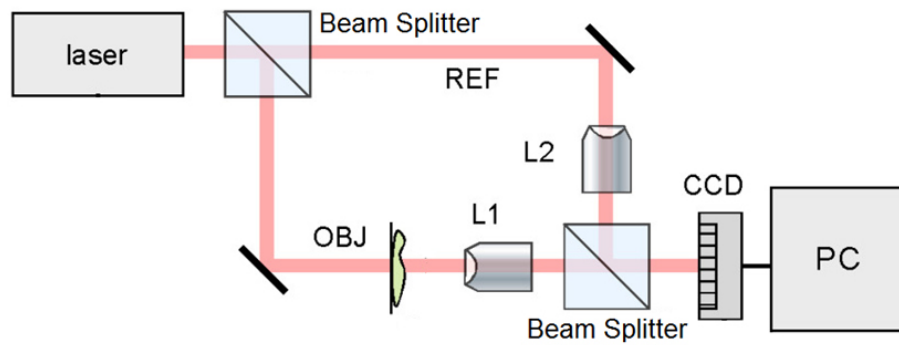


Figure 1.1 Illustration of digital holographic microscopy system (Mann et al., 2006)

After getting digital hologram, image is reconstructed in computer via a reconstruction algorithm. For getting holographic images, a monochrome light source such as laser is used. Main advantage of digital holography is capable of recording 3D volumetric field information on a single hologram with 5nm accuracy. As a result of this, only one CCD sensor is needed. On the other hand, reconstruction of image can be slow. Time of reconstruction process depends on selected algorithm, optical setup and hardware. Also the systems contains expensive elements which makes digital holographic microscopy method rarely found.

Another 3D motion detection method is micropillar based PDMS (Polydimethylsiloxane) device (Ghanbari et al., 2012; Held et al., 2009; Sheng et al., 2006). In this system, motion of microorganisms are detected by micropillars mounted on the surface (Figure 1.2, 1.3).

Micropillar based PDMS device is formed as a pillar matrix. Micropillars

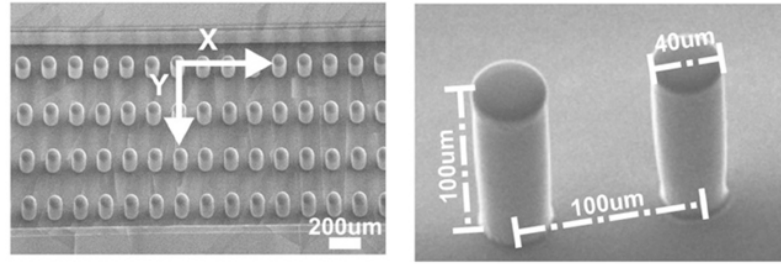


Figure 1.2 Inside of Micropillar based PDMS device (Ghanbari et al., 2010)

work as force transducer. They generate electrical signals according to force on them. Advantages of PDMS are its transparency, flexibility, biocompatibility and very sensitive measurements. However manufacturing process is too complex and expensive.

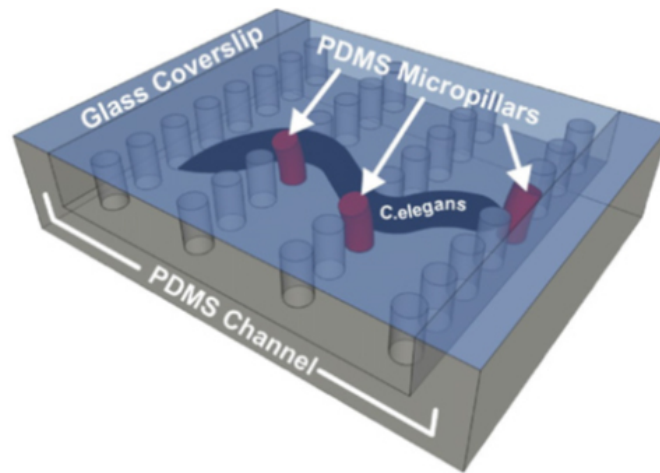


Figure 1.3 Illustration of Micropillar based PDMS device on work (Ghanbari et al., 2010)

3D Motion Tracking is not only used for small organisms but also bigger objects such as ball. Hawk-Eye technology was developed for cricket sport by Hawk-Eye Innovations Ltd. (Winchester, Hampshire). Also it has been used for other sport organizations such as tennis (for seven years), and football (for two years). The main goal of the system is detecting line crossings in critical moments. The results can be seed at 3D visualised animations. Also it stores data to provide the graphical representation of statistics after match.

The system's working principle is based on very fast video processing from multiple calibrated cameras (Figure 1.4). Firstly, the pixels belong to ball is isolated from other

objects. In this step, 2D coordinates of ball's center of mass is detected by each camera separately. Also lines and other objects are defined by image processing algorithms. After that, obtained coordinate values are combined to generate 3D position of the ball. The values of calibration set-up are used to obtain real world positions correctly with 3.6mm. accuracy. This process is repeated continuously at speed of 1000 fps so that the 3D positions of the ball can be combined to produce a single trajectory of the flight of the ball (Hawk-Eye Innovations Ltd., 2014).

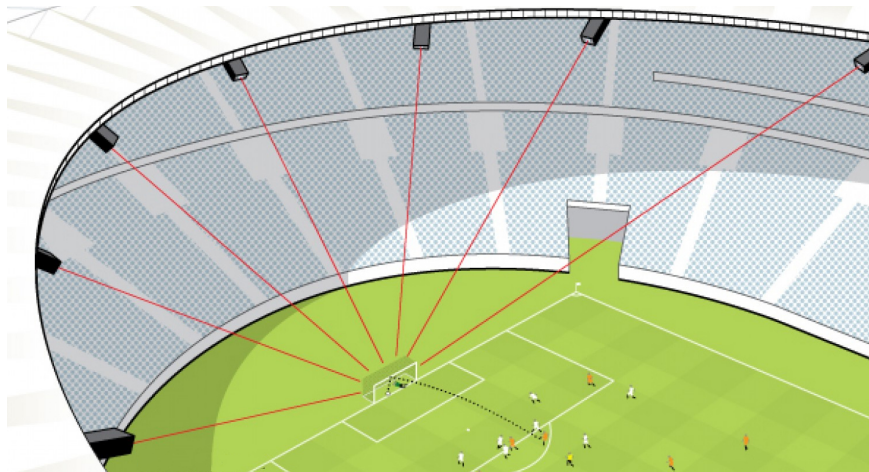


Figure 1.4 Working principle of Hawk-Eye system football (Visual.ly , 2014)

Using digital cameras is also preferred for motion tracking of organisms (Alyuruk et al., 2013; Kokkali et al., 2011). There are some advantages and disadvantages of this approach. The main disadvantage is that it cannot produce similar precisely results as digital holographic microscopy and Micropillar based PDMS device. However this level of precision is not necessary for tracking motions of *Artemia salina*. The major advantage of this system is that it does not include fairly expensive and complex components with respect to other methods. Also, they can be found on market easily. Furthermore digital cameras can give results faster than other methods.

In previous works (Alyuruk et al., 2013), only survival percentage, velocity and paths covered by *Artemia salina* were examined. However, this project includes more detailed and precise motion analysis. This analysis were handled by an autonomous algorithm with help of new used features.

There must be two or more cameras to perform an efficient 3D motion detection

and analysis. Our proposed system consists of two digital cameras. Moreover, the system produces successful and fast results according to its set-up. All the details of this system will be given at 3D Video Capture System section.

1.2 Stages of the Project

This project consists of four steps; preparation of *Artemia salina* larva, stereo recording, object detection and tracking, motion feature extraction and classification (Figure 1.5).

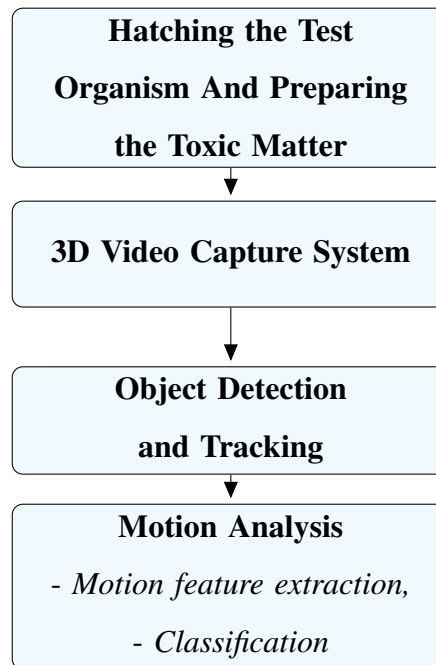


Figure 1.5 Sections of the system

All *Artemia salina* nauplii were produced under the same conditions just before each testing procedure. Their motion in different molarity of potassium dichromate (a kind of a toxic matter (Kusk & Nyholm, 1992)) diluted in salty water were recorded by 3D vision setup. Afterwards, 3D Cartesian coordinates of *Artemia salina* were extracted from video files. Characteristics of motion were analysed and classified. Type of the motion and time parameters were used for indicating the toxic molarity of the solution.

CHAPTER TWO

HATCHING THE TEST ORGANISM AND PREPARING THE TOXIC MATTER

Life cycle of *Artemia salina* has diverse stages from hatching till adulthood (Figure 2.1).

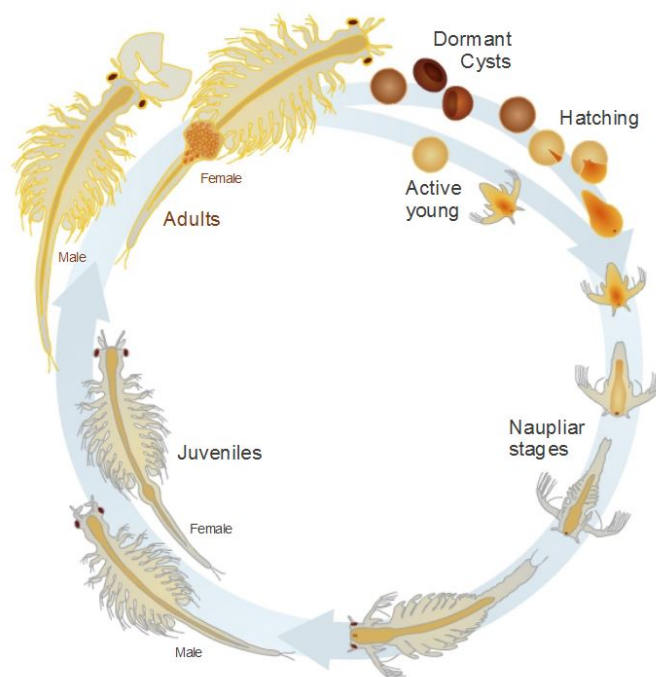


Figure 2.1 Life cycle of *Artemia salina* (Learn Genetics, 2014)

It starts from dried cysts. In nature, hatching process begins after winter when water temperature comes to enough stage. With trigger of temperature, cysts become bursting and embryo appears (Figure 2.2).

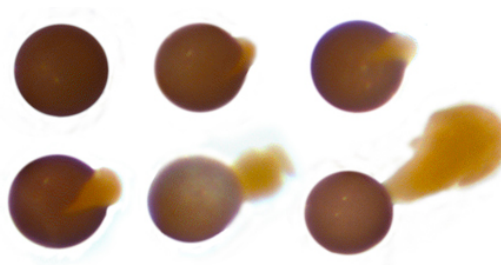


Figure 2.2 Hatching of *Artemia Salina* (Learn Genetics, 2014)

After hatching, *Artemia* larva is at naupliar stages (Figure2.3). At this point, growing of *Artemia salina* launches. These stages are very significant for the response

of *Artemia* to toxic matter. At first stage, *instar I*, larvae are fed from cyst and are not in contact with the medium so much. After the food in the cyst run out, they start to feed from external resources in the water. Thus, *Artemia* should be used for toxicity test at *instar II-III* stage since this is the most toxic-sensitive stage (Sorgeloos, 1978). Due to this fact, hatching procedure for all testing applications was done under strict rules and same conditions to obtain nauplii in determined stage.

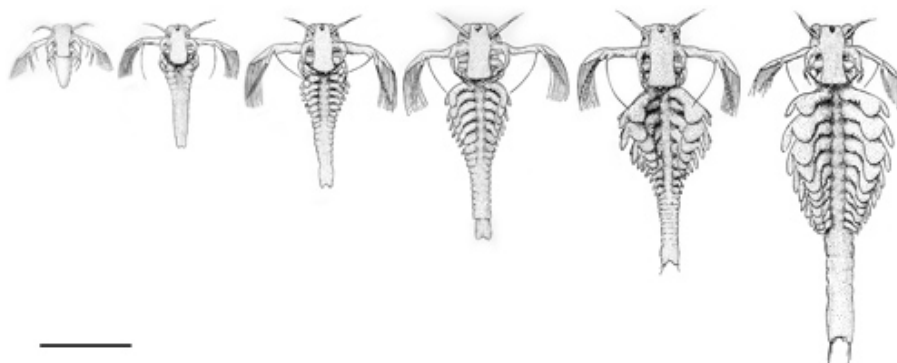


Figure 2.3 Naupliar stages of *Artemia salina* between instar I and VI (Heath, 1924)

In this project, the commercial *Artemia* cysts produced in the Great Salt Lake were preferred. Artificial seawater was prepared with local and chlorine free water. 35 g/L *NaCl* added to water and mixed. Spring or aquarium water was not used since higher pH level is advised by manufacturer for hatching. *Artemia* cysts were put in a 50 ml falcon tube and saline water added. Also, air bubbles were supplied to falcon tubes to get a continuous movement of cysts (Figure 2.4). Falcon tubes were placed in an illuminated aquarium. The most important point was to keep the temperature of the water at the same level (24°C in this project) during hatching since water temperature dramatically effects speed of hatching process which is strictly relevant for stages of nauplii (Sorgeloos, 1978).

In 24°C medium, *Artemia salina* reach instar II-III at 48 hours from beginning of hatching process. At this stage, *Artemia* nauplii were taken from falcon tube into an observation cuvette. *Artemia* nauplii were observed under different concentration of potassium dichromate ($K_2Cr_2O_7$) diluted in artificial seawater. In addition, another set of nauplii recorded in potassium dichromate free artificial seawater was used as control group.

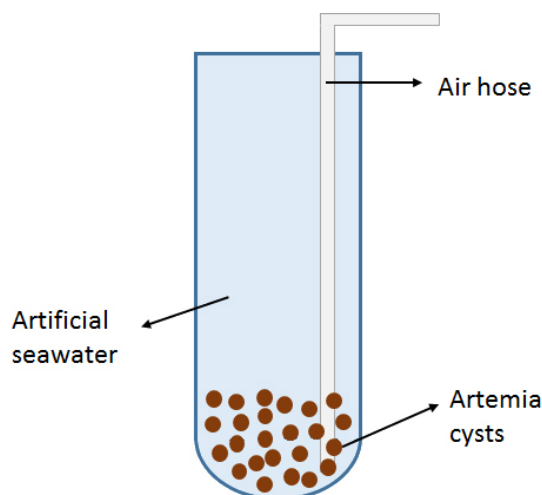


Figure 2.4 Illustration of hatching tube

A stock solution at concentration of 1000 mg/L potassium dichromate was prepared. Fresh solutions were diluted from stock for each observations just before experiments. In this project, the motions of Artemia were analyzed at 100 mg/L, 125 mg/L, 150 mg/L, 175 mg/L and 200 mg/L concentrations. Also same test procedure were applied a control group that observed in artificial seawater without $K_2Cr_2O_7$

Motions of 20 different Artemia nauplii were analyzed for each concentration and control group. 120 different nauplii were used totally. In addition, tests were performed in four different sessions for each case to show the time independence of the system.

CHAPTER THREE

3D VIDEO CAPTURE SYSTEM

3D Video Capture System in this thesis consists of two main parts: hardware and software. 3D video of *Artemia salina*'s motions was captured by industrial cameras and by the stereo vision software that we have developed.

3.1 Capture System Hardware

3.1.1 Hardware Set-up

The components of the system were rails, transparent cuvette, two cameras with two lenses, led matrix and computer. Rails were connected to a hard plastic surface and other elements were attached to rails. Rails gave opportunity to instant modifications on the set-up (Figure 3.1).

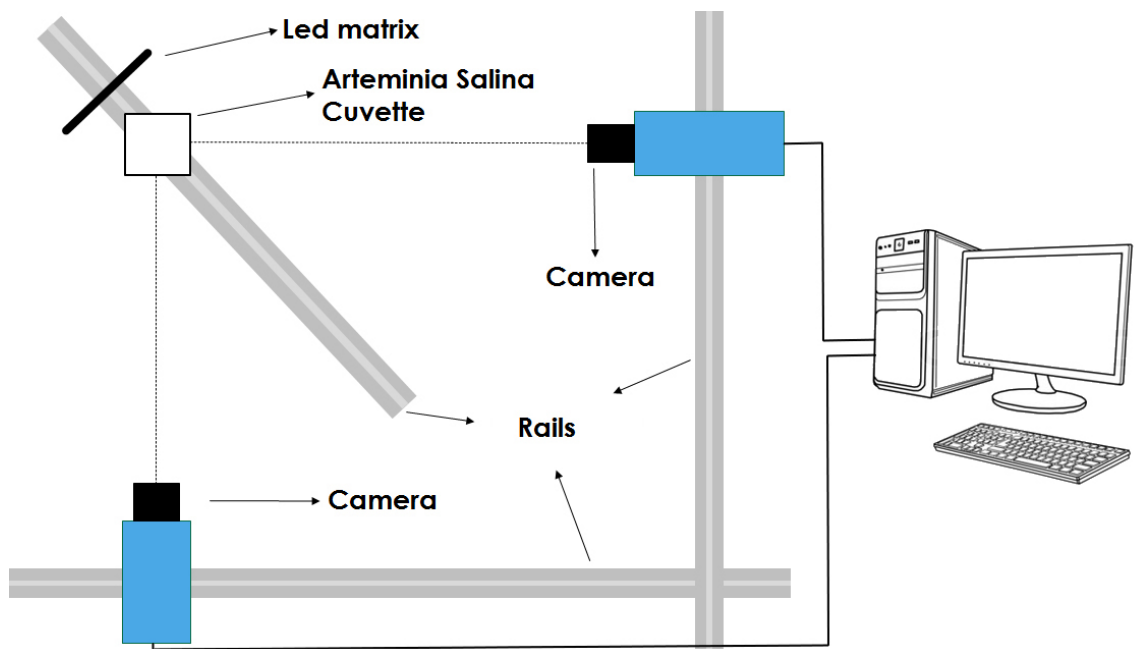


Figure 3.1 Illustration of sytem set-up (top view)

Two cameras were mounted at a plane with 90° angle with respect to the each other. With the help of this placement, (x,y,z) coordinate values of organisms were determined.



Figure 3.2 Picture of sytem set-up

In this configuration, one of the camera was chosen as a master, while the other one was as a slave. Master camera provided the (x,y) values of the position. Slave camera gave the (y,z) axis value with respect to master camera. Y-axis values of both cameras matched with each other and according to this match, z value was obtained from slave camera.

Motions of *Artemia salina* were examined in a square 10 mm x 10 mm x 45 mm fully transparent disposable cuvette.



Figure 3.3 10 mm x 10 mm x 45 mm macro cuvette

LED array was mounted to a concave shaped surface for lighting the cuvette. More than 120 LEDs were mounted to provide bright white light. LED array was placed

outside from cameras' field of view to avoid overexposed images. Whole system was enclosed by a cover to block other light sources.

3.1.2 Camera

For 3D motion detection and analysis fast, precise and accurate stereo vision is needed.

Artemia salina is a fast moving microorganism. Also it has complex types of motions. Because of these, we needed a camera with fast capture capability. Additionally, capturing from two RGB video with higher frame rate needs wide-band connection interface.

Furthermore, stereo vision also needs a requirement for absolute synchronization. This kind of precisely synchronised recording is very hard by software trigger because there sending the *start* command to two independently connected different devices by the software at the exactly same time need special modifications and optimizations.

According to these essential circumstances, an industrial GigE camera, DFK 23G618 from The Imaging Source Europe GmbH (Bremen, Germany), was chosen. This model can capture 640x480 RGB videos at 120 fps. GigE interface enables up to 1000 Mbit/s data transfer speed. It can be triggered by software or externally. Some important specifications of DFK 23G618 is shown at Table 3.1. (All the specifications can be downloaded from: archive.theimagingsource.com/en_US/p/c7374d74/)

It was observed that 640x480 Y800 (monocolor) 90 fps recording satisfies all necessary conditions in this project. Capturing with more fps or in RGB color cases were not preferred because they hold more and unnecessary space on storage device. Reasons of these preferences will be discussed in Video Capture System Software section.

Two cameras were connected to two separate Pci-e 1 Gb/s Ethernet cards with two separate cables. Using one Ethernet with card two input or a data switch/hub was not

Table 3.1 Specifications of DFK 23G618 (The Imaging Source, 2014a)

Video formats @ Frame rate	640x480 RGB32 @ 120, 90, 60, 30, 15, 7.5, 3.75 fps 640x480 Y800 @ 120, 90, 60, 30, 15, 7.5, 3.75 fps
Dynamic range	8 / 12 bit.
Resolution	H: 640, V: 480
Pixel size	H: 5.6 μm , V: 5.6 μm
Interface	GigE
Shutter	1/100000 to 30 s
Trigger	Software or External
Size	29 x 29 x 57 mm
Lens type	C and CS mount lenses
Software Development Kits	IC Imaging Control .NET Component, IC Imaging Control C Library

opted to prevent sharing the bandwidth. On the other hand, static IP numbers had to be defined and IP configurations had to be done manually. Otherwise, there were IP number conflicts if they were arranged automatically. IP configurations were defined by GigECam IP Configuration software provided by manufacturer (Figure 3.4).

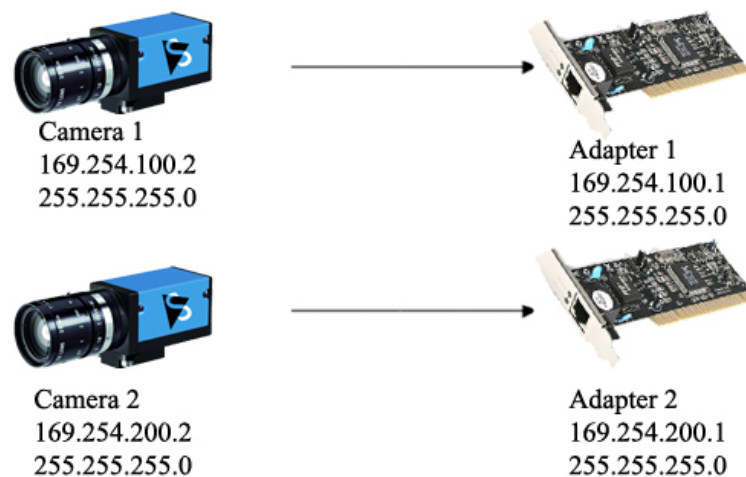


Figure 3.4 Static IP configuration of cameras (Advanced Vision Technology , 2014)

The first and second section of IP numbers are same however other parts have to be different. Third section defines group and it must be same number for each Ethernet

The diagram shows the rear panel of the 1000 Series Laser Module with the following pinout labels:

- 1:** +12VDC (+/- 10% max.)
- 2:** Trig +
- 3:** Trig -
- 4:** GPO_OUT (Strobe) (Open Drain output)
- 5:** GPO_GND (Open Drain output)
- 6:** GND_DC
- Notch:** Points to the notch in the connector housing.

DFK 23G618 has two ports, Ethernet and I/O socket. Power and external trigger were connected at this I/O socket (Figure 3.5).

[illegible]

calculated according to delay and exposure times of camera (Figure 3.7).

14

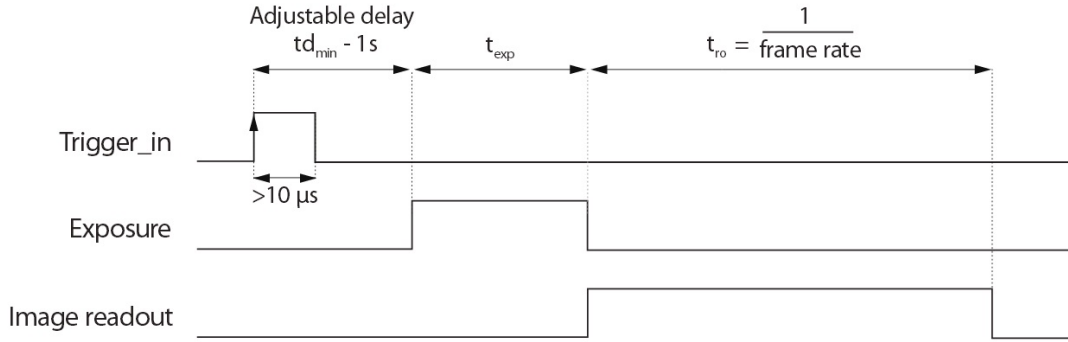


Figure 3.7 Timing diagram of DFK 23G618 (The Imaging Source, 2014b)

of DFK 23G618 is $4 \mu s$. According to these values period of trigger circuit was tuned for 90 fps video capturing.

3.1.3 Lens

Selecting lens was another critical decision in this system. Firstly, the position and distance between cuvette and camera was determined. A closer placement provides a clear and zoomed images. However only a small portion of the cuvette is usable in this condition. Also focusing on each location of cuvette is very difficult because effective focal length dramatically decreases in closer placements. In addition to them, higher perspective effect happens in this situation.

In contrast with that, another option is the far placement. In this case perspective and focusing problems are not happen but *Artemia salina* is a small microorganism and it is hard to observe it from a far distance.

The position of cuvette was determined to 30 cm from cameras. This place was not close to camera also not far too. In this situation 10 mm x 10 mm x 25 mm of cuvette could be usable. Other parts were out of view. Despite of this loss, there were no critical perspective and focusing problems. Details of them will be discussed at Calibration of Set-up section.

After deciding position and other specifications, lens model was chosen as Tamron

M118FM25 (Figure 3.8, Table 3.2).



Figure 3.8 Picture of Tamron M118FM25 (Tamron, 2014)

Tamron M118FM25 is produced to use with industrial cameras in a compact size. Its has adjustable and wider aperture which supplies more light to camera sensor. Also, 25 mm focal length is suitable for our needs.

Table 3.2 Specifications of M118FM25

Focal Length [mm]	25
Maximum Aperture	1.6
Focus	Manual
Mount	C
Filter size [mm]	25.5

3.2 Calibration of Set-up

All the components of the system were mounted carefully. Many measurements were taken. Two cameras, platform of cuvette and LED matrix were hold with capscrews. The alignment of cameras were corrected with help of live view feature of stereo recording software.

Also a chessboard image (Figure 3.9) was used to test the system about perspective effect and focusing which are discussed in Lens section.

A 10 mm x 10 mm chessboard image was printed as a test image. Firstly it was attached to in front of cuvette and a sample image was taken. After this it was attached

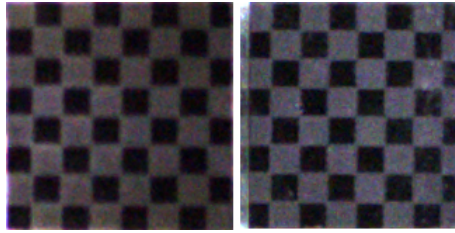


Figure 3.9 Chessboard images taken from in front of and back of cuvette.

to back of cuvette and same procedure was done. It was observed that, there was no critical distortion or focusing problem at any part of the cuvette. The only problem was that, there was some image loss at the left/right edges of back image. The reason of this problem was induced by thickness of transparent cuvette's wall. This situation caused a few fragments in motion tracing process if *Artemia salina* was at the edges of cuvette. Fortunately this problem happened barely and in most cases the fragments could be filled by interpolation. As a result, it did not defect the system performance critically.

3.3 Video Capture System Software

After completing hardware set-up of the system, it was required to develop a stereo video capture software. Fortunately, Imaging Source Europe GmbH provides a powerful software development kit (SDK). This SDK includes many basic functions and some samples written by C++, C, VC++, C# and ActiveX languages. C# is a practical and efficient platform so Microsoft Visual C# Express 2010 and C# was selected to develop the stereo recorder software.

Region of interest (ROI) was defined to capture only cuvette part. There was no need to full frame capturing and cropping. Users can adjust dimensions and position of ROI via software. Before starting capture, all the options can be set while live view is active. This feature provides user to observe effects of the preferences before capture process.

On the other hand, the SDK provides a detailed camera settings user interference.

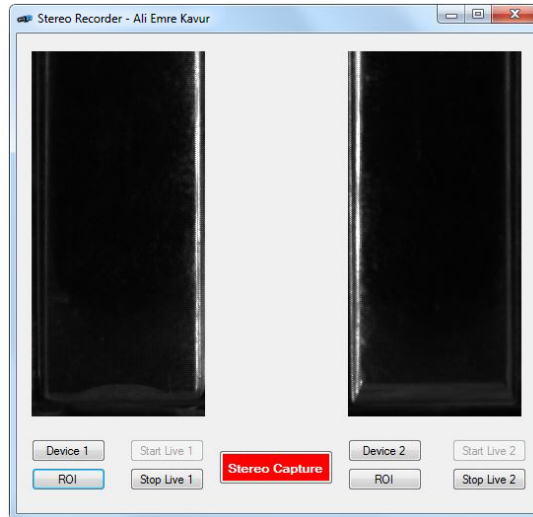


Figure 3.10 Stereo Recorder Software

White balance settings for each color, exposure time, sensor gain, trigger options, frame rate, video format can be defined by this sections (Figure 3.11).

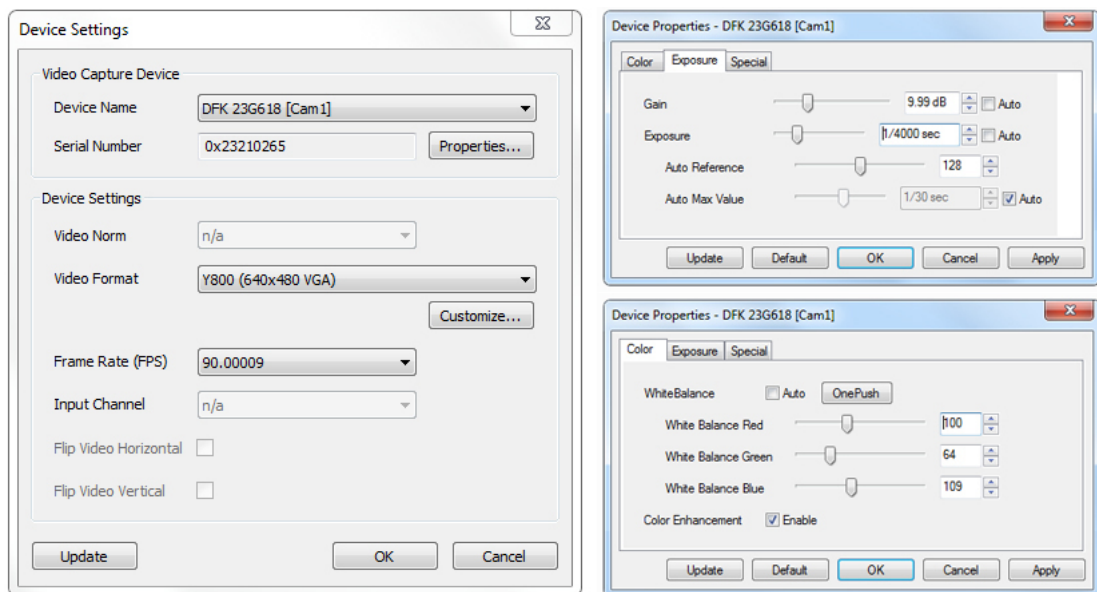


Figure 3.11 Camera settings sections

In this project white balance, exposure time and sensor gain of camera settings were determined by trial and error method. An optimal and balanced settings had to be selected to take clear and meaningful video frames. For example, more sensor gain brings more noise. Also more exposure time may cause over-saturation or vice versa. Color of *Artemia salina* is closer to orange so more intense white balance for red

and blue were preferred. On the other hand, the color of the medium in the cuvette changes for different concentrations. For example, color of 200 mg/L potassium dichromate solution is yellow while non-toxic solution is transparent. Color settings were optimized for each case to get most beneficial images.

Any compression was not done while recording videos because compression process needs more CPU power and causes defecting frames during simultaneous recording. Y800 (8-bit grayscale) video format was selected (Figure 3.12).

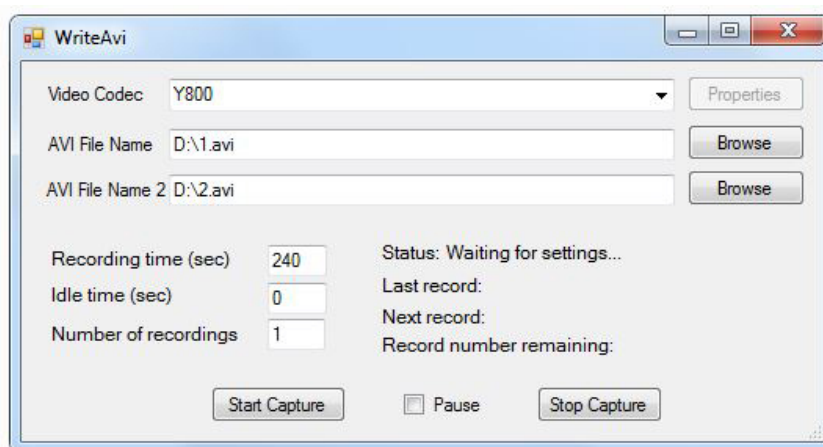


Figure 3.12 Recording settings window

In addition with these, there were another options designed for users. The recording software is capable of working iteratively. Recording period, number of recordings and idle time between recording sessions can be defined. As a result of these, users can take video captures in same periods automatically.

Starting capturing was a two step process. Firstly user started the recording from the software interference. After this command, software was waiting the trigger signal from trigger circuit. User started the circuit and trigger pulses sent to the cameras simultaneously. Cameras snapped frames and sent it to PC at the same time. This two steps procedure guarantees the absolute synchronization.

Video capturing process was dealt with a PC under Windows 7 operating system. The PC consisted of AMD Phenom II X4 CPU, 8 GB of RAM and 128 GB Kingston solid state drive (SSD). Two simultaneous and non compressed video capturing needed

too much bandwidth. Sometimes it was observed that, writing speed of a hard disk drive was not adequate for it due to fragmentations on disk. Because of this, video recordings were taken to directly SSD. After finishing video capture process, videos were compressed to save storage volume. Compression procedure was handled with Matlab software with H.264 codec. Without any distortion, data size of a video file was decreased to %10 of original file after compression.

CHAPTER FOUR

OBJECT DETECTION AND TRACKING

There are many basic or sophisticated approaches for detecting the position of the moving object from continuous frames. The most simple way is selecting a previous frame far of the current frame as background and subtracting it from corresponding frame. The obtained image is converted to binary image according to a given threshold. In result images, the true pixels are belong to the moving object while zeros are background. Mathematically

$$F_{n(x,y)} = \begin{cases} 1, & I_{(x,y)} - B_{(x,y)} > t \\ 0, & \text{otherwise} \end{cases} \quad (4.1)$$

where $F_{n(x,y)}$ is current output, (x,y) are coordinates of the pixel, I is current frame, B is background frame, t is threshold.

This method is easy but not always successful. Even a smaller noise may corrupt results. In this project, an effective and robust algorithm, approximate median method was applied to video pairs to detect the Artemia's position (McFarlane & Schofield, 1995). This method is suitable for detecting objects which are very smaller than total field of view and have no differentiable borders. Also, it is resistant to discontinuous noises. (McFarlane & Schofield, 1995)

The difference between the approximate median algorithm and typical background subtraction method (Equation 4.1) is the construction of the background image (Equation 4.3). In the approximate median procedure, background image is updated at each iteration according to the rule: if a pixel in the current frame has a value larger than the background pixel, the background pixel is incremented by 1. In a similar manner, if the current pixel is less than the background pixel, the background is decremented by 1.

$$F_{n(x,y)} = \begin{cases} 1, & I_{n(x,y)} - B_{n(x,y)} > t \\ 0, & otherwise \end{cases} \quad (4.2)$$

$$B_{n+1(x,y)} = \begin{cases} +1, & I_{n(x,y)} > B_{n(x,y)} \\ -1, & I_{n(x,y)} < B_{n(x,y)} \end{cases} \quad (4.3)$$

where $B_{n+1(x,y)}$ is background of next iteration, $B_{n(x,y)}$ is current background.

After some iteration, background converges to the image which contains only static objects, not any moving objects (Figure 4.1). Briefly, approximate median method gives very accomplished results without using a complex algorithm and high resources.

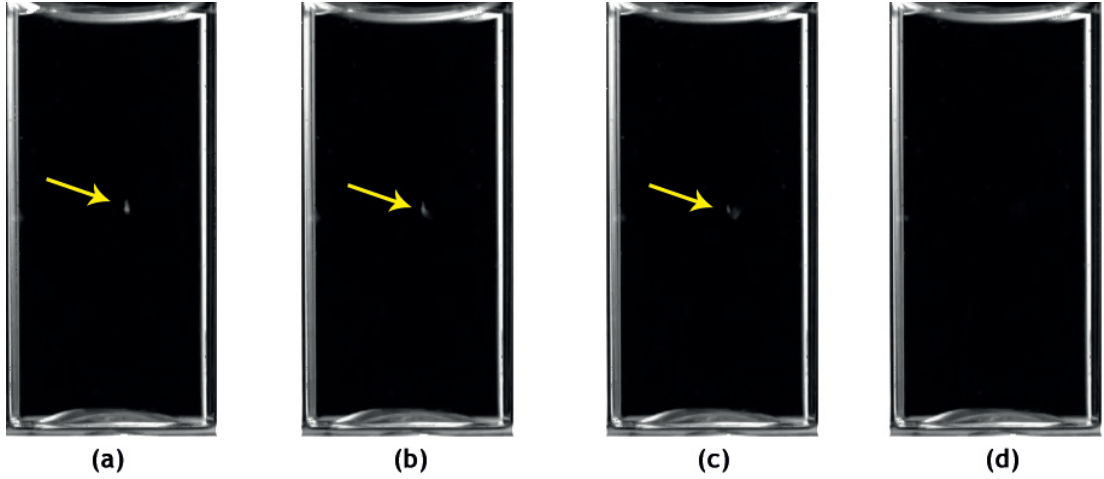


Figure 4.1 Background images produced by the approximate median algorithm (a) at 1st iteration (pixels of nauplius is pointed by yellow circle), (b) at 30th iteration, (c) at 60th iteration, (d) at 90th iteration, there is no pixels of moving object any more.

Erosion and dilation process were applied sequentially to the output of approximate median function. Basically erosion is a process that peels the boundary pixels of binary object. The size and shape of peeling is determined by structure element. Dilation is the reverse process of erosion. The structure element of erosion and dilation were used as 2x2 square operator. Sequential usage of erosion and dilation was used to eliminate noises that came from camera sensor. Resulted image contained only pixels of organism. Coordinates of objects was defined by only one pixel value which is positioned at the objects center of mass. After determining the positions of the nauplii at each video pair, the next step is to match coordinates in order to obtain 3D position

values. The first camera was defined as master while other one was slave. Frames from master camera gave the X-Y coordinates of the object while depth information (Z axis value) was obtained from slave camera. Y axis values of the object are corresponded in each video pair in this set-up. This feature was used to match coordinates with combination of all these data, 3D Cartesian coordinates of the nauplius were extracted. Figure 4.2 shows the some sample trajectories of one nauplius in different times. It can be seen that *Artemia Salina* has various motion characteristic.

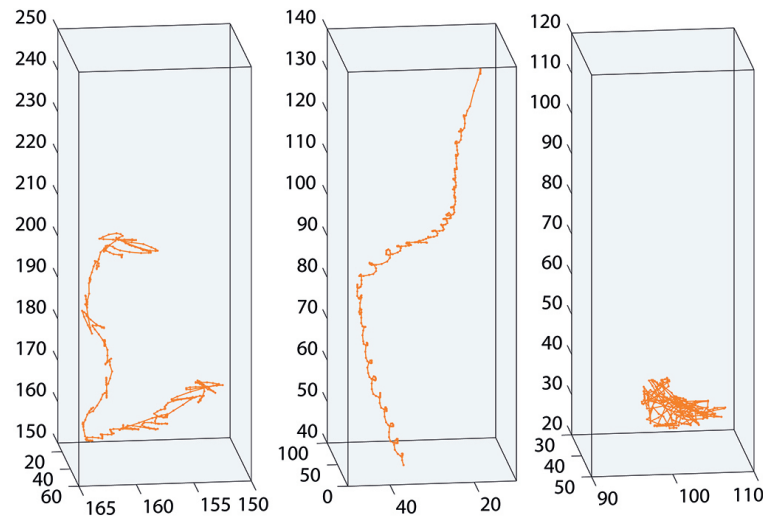


Figure 4.2 Some motion samples of *Artemia* nauplius during 4 seconds

There might be some uncertain errors such as a little swinging during the video capturing process. To handle this problem, motion pattern is barely smoothed to reduce errors. Smoothing algorithm was decided as LOESS (Local Regression Smoothing) method (Loader, 2004) with span value 1 because of its efficiency and simplicity. Basic principle of LOESS is that a smooth function can be well approximated by a low degree polynomial in the neighbourhood of any point in input. There is no global assumptions about the input but it is assumed that it can be well approximated with parametric function locally.

Figure 4.3 shows the trajectory before and after smoothing process. As it can be seen at the figure, the smoothing process was not changed the trajectory completely. However it was improved performance of classification by eliminating smaller distortions.

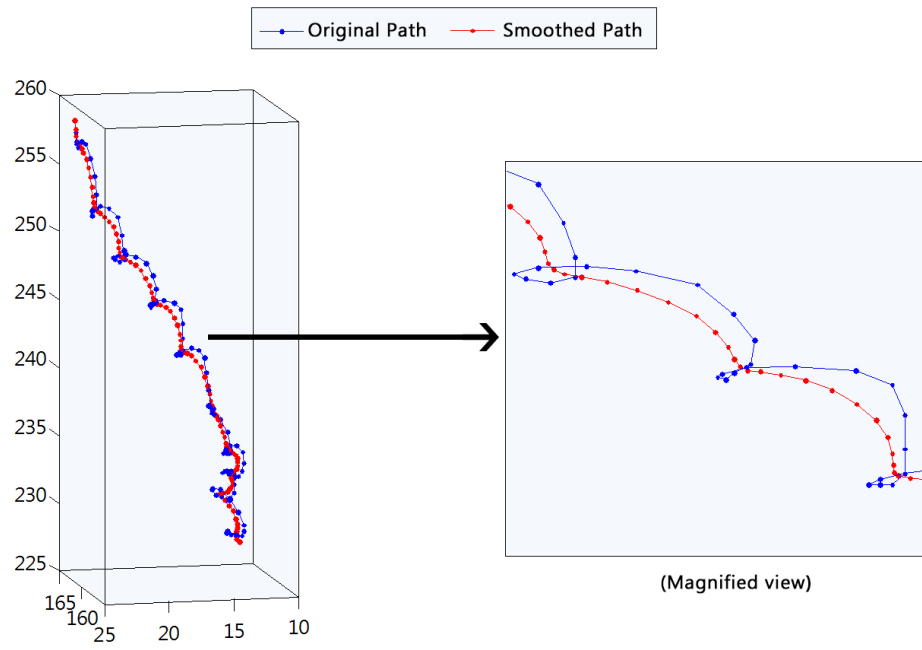


Figure 4.3 Results of smoothing on motion paths.

CHAPTER FIVE

MOTION ANALYSIS AND CLASSIFICATION

In this chapter, all the details of features extractions and motion classification for motion trajectory analysis are given. Movement of *Artemia salina* is a combination of linear and helical motion which is similar to human sperm motion. Therefore, some features such as curvilinear velocity, average velocity, straight line velocity, linearity, wobble (Mortimer & Mortimer, 1990; Geyter & Geyter, 1998) were used to analyse the motion of *Artemia Salina* in toxic environments.

To do this, motion paths were divided into 4 seconds of tracking windows (therefore we have 4 seconds x 90 fps = 360 3D coordinate points for each window since fps is 90). Duration of the windows was determined by trial and error method. In larger windows, motion types mix with each other. Inversely, the detail of information was missed in smaller windows. Also these 4 seconds of tracking windows were separated and analysed with one second of sub-windows. The reasons and effects of these preference will be discussed at the Motion feature extraction and Classifier sections.

5.1 Motion Feature Extraction

1. Curvilinear velocity (V_C) was derived by Euclidean distance between all sequential points in the tracking window. Velocities were acquired by division distances of time.(3) Average of all V_C values between sequential points in a tracking window was accepted the velocity of the window (5.3).

$$D_i = \sqrt{(x_i - x_{i+1})^2 + (y_i - y_{i+1})^2 + (z_i - z_{i+1})^2} \quad (5.1)$$

$$V_{Ci} = \frac{1}{\Delta t} D_i \quad (5.2)$$

$$V_{Cwindow} = \frac{1}{n} \sum_{i=1}^n V_{Ci} \quad (5.3)$$

where x, y, z are 3D Cartesian coordinate values, n is number of points in the window, Δt is the time duration of window.

2. Average velocity (V_A) was similar to V_C . However, the motion pattern was smoothed moderately by LOESS method to obtain an average path before calculation. After this, V_A was acquired by the same procedure as V_C .

3. Straight line velocity (V_S) was obtained from the distance between first and last point in tracking window. It shows the Artemia's change of location. It is independent from the shape of movement pattern.

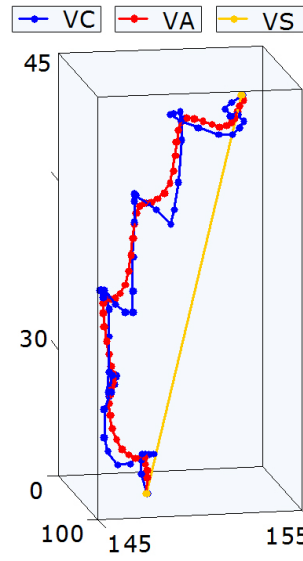


Figure 5.1 Illustration for calculation paths of V_C , V_A , V_S

4. Linearity (L) is a parameter that indicates straightness of the motion pattern. It was determined by ratio of straight line velocity and curvilinear velocity.

$$L = V_S / V_C \quad (5.4)$$

5. Wobble (W) defines tortuosity of the trajectory. Higher wobble means that object moves in roughly changed shaped pattern while lower wobble means that there is a smooth shape. Wobble was computed by V_A , V_C values with the following equation:

$$W = V_A / V_c \quad (5.5)$$

6. Fractal dimensions (D_f) concept was adapted as a feature too. Basically, fractal dimensions is a ratio that implements statistical value of complexity in a

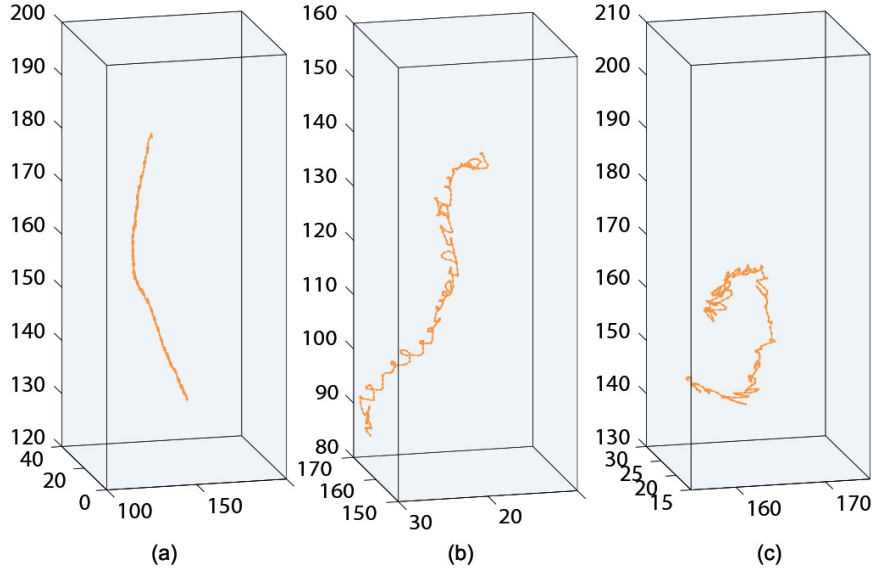


Figure 5.2 Different L and W combinations samples: **(a)** Higher L (0.632) and lower W (0.514) **(b)** Higher L (0.574) and higher W (0.584) **(c)** Lower L (0.215) and higher W (0.643)

pattern. Unlike Euclidean dimensions, fractal dimensions can be non-integer value. Complex patterns have higher fractal dimension value while smooth ones are lower. The difference between wobble and fractal dimension is that, wobble is helpful for determining local changes in the motion pattern. On the other hand, fractal dimensions examines whole pattern at once. This is useful for analysing pattern completely. This speciality was used as a feature for examining tortuosity of patterns (Dickle & Burrough, 1988). To the best of our knowledge, this is the first work that uses fractal dimension concept as a motion feature. There were several ways to calculate the fractal dimensions. In this study, box counting method was preferred. Box counting method is the ratio between number of boxes($N(r)$) and size of boxes r to cover all of the shape.

$$\dim_{\text{box}} = \frac{\log N(r)}{\log(1/r)} \quad (5.6)$$

In some type of notations, $1/r$ is accepted as magnification factor. As the other features, fractal dimensions were calculated for each tracking windows too.

In our observations, it was detected that average velocity, curvilinear velocity, straight line velocity were not distinctive features separately (Figure 5.3). On the other hand, wobble and linearity were very valuable for pattern classification. Due to this fact, V_c , V_A , V_S were not used as a feature directly. They were used to calculate W and

L .

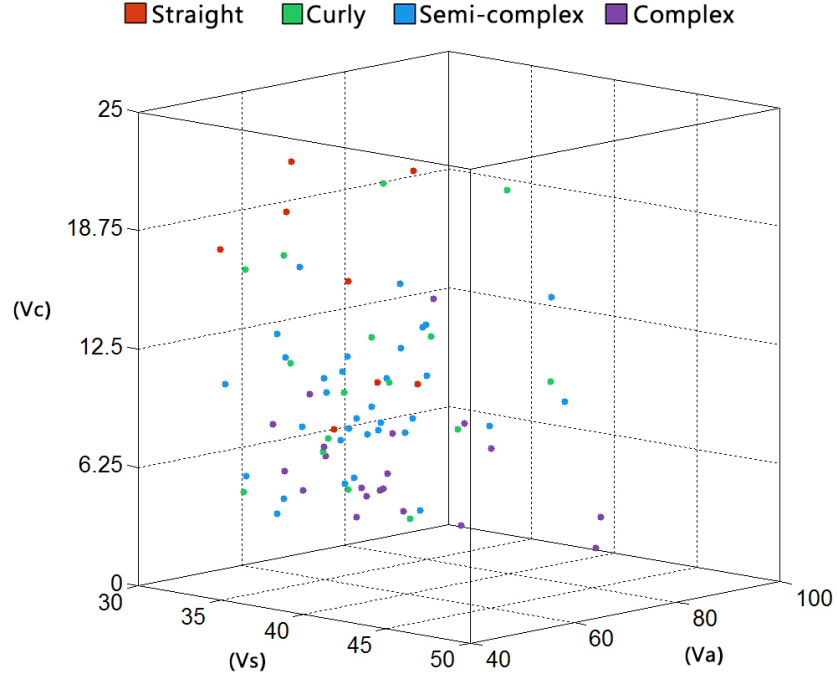


Figure 5.3 Distribution of V_c , V_A , V_S according to motion types. It can be observed that V_c , V_A , V_S are not distinctive features.

Beyond them, all of the features were calculated for one second (90 points) of sub-windows. $(L_{sub}, W_{sub}, Df_{sub})$ This approach was useful for determining stability and homogeneity of motion during 4 seconds of tracking. These sub-features were not used as independent features. The difference between maximum and minimum of them in a main tracking window was calculated for each same type of feature. For example, L_{W_i} is value of linearity for a tracking window (W_i). Also $L_{W_{i-1}}, L_{W_{i-2}}, L_{W_{i-3}}, L_{W_{i-4}}$ are linearity values for each sub-windows of W_i . L_{subW_i} is calculated by:

$$L_{subW_i} = \max(L_{W_{i-n}}) - \min(L_{W_{i-n}}), \quad (5.7)$$

$$n = 1, 2, 3, 4$$

These additional sub-features helped to determine the similitude of main feature during tracking window. Lower values indicated that the feature value of main window covers whole window. However, higher values pointed out that motion pattern is different at some sections of the main window. This method contributed distinguishing

semi-complex patterns from fully complex ones and it increased performance of classification process.

To sum up, six features (L , W , Df , L_{sub} , W_{sub} , Df_{sub}) were used for each tracking window totally.

5.2 Motion Classification

5.2.1 Motion Classes

Motions of *Artemia salina* was investigated into four groups according to their movement shape. These four group was determined by our observations. Significant changes of motion, ability to classification and sensitivity for toxicants were taken into account. Displacement, motion shape and tortuosity were the key factors for separating groups.

1. Straight (Group 1) covers linearly motions. Object does not make zig-zag or helical actions. Its aim is to get maximum displacement. However there might be a very few curvy acts.

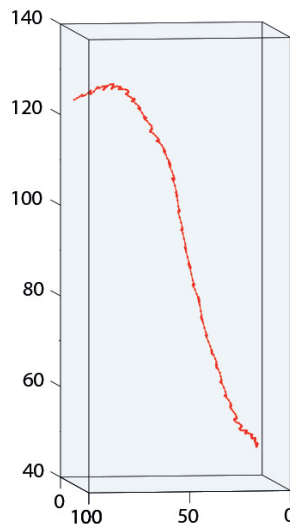


Figure 5.4 A sample of straight motion

2. Curly (Group 2) contains less straight motion than group 1. Object attempts displacement again but it makes some helical acts without rough changes. That means motion is smoothly curvy.

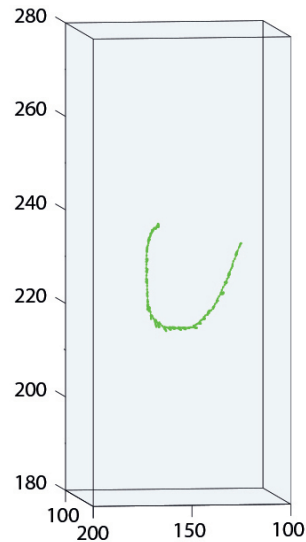


Figure 5.5 A sample of curly motion

3. Semi-complex (Group 3) includes more helical and curvy motions. Object makes few displacements but zig-zag patterns occurs more.

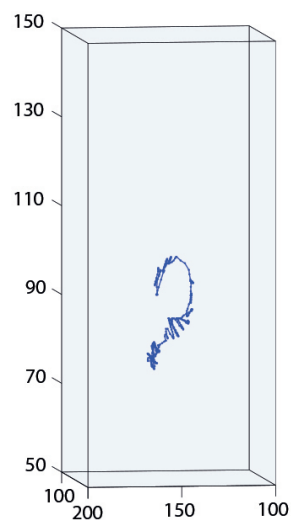


Figure 5.6 A sample of semi-complex motion

4. Complex (Group 4) covers complex movements. Motion pattern is dominated

by tortuosities. Nearly there is no displacement. Also shape of many acts cannot be distinguished by human vision without zoom.

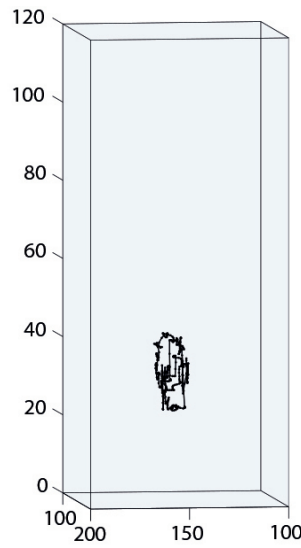


Figure 5.7 A sample of complex motion

5.2.2 Classification Method

50 motion samples for each motion type were picked and defined manually. Figure 5.8 shows the relations between motion types and features L , W and Df . It was observed that the features were not linearly separable. As a result of this, an artificial neural network based classifier was designed to determine groups. Artificial neural network (ANN) is a computational model inspired in the natural neurons. ANN basically consist of inputs, which are multiplied by weights, and then computed by a mathematical function which determines the activation of the neuron. Another function computes the output of the artificial neuron. ANN must be trained with train data for once. Training process constructs weights. After this, ANN is ready to classify the input.

50 samples from each motion type (total 200 samples) were divided into training (%70), validation (%15) and test (%15) groups for neural network based classifier.

The ANN (Figure 5.9) contains two layers, hidden and output. Hidden layer has

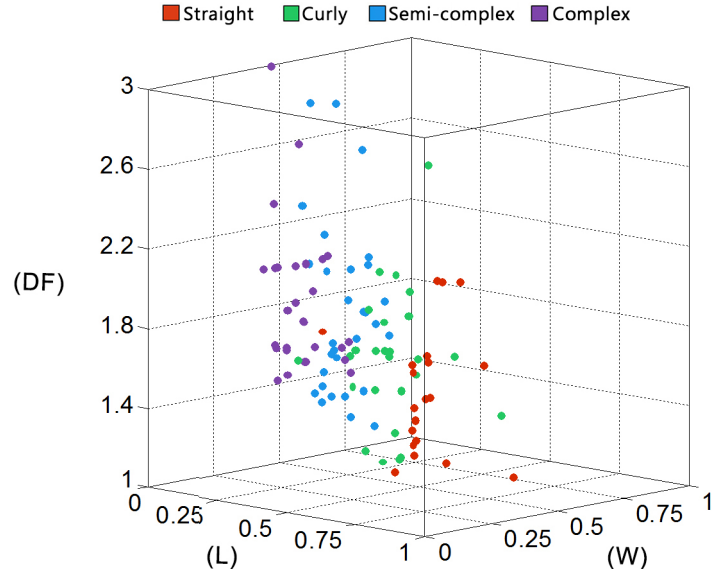


Figure 5.8 L , W and Df values coloured according to motion types.

six neurons. Transfer function of them is hyperbolic tangent sigmoid transfer function. Furthermore, output layer has four inputs.

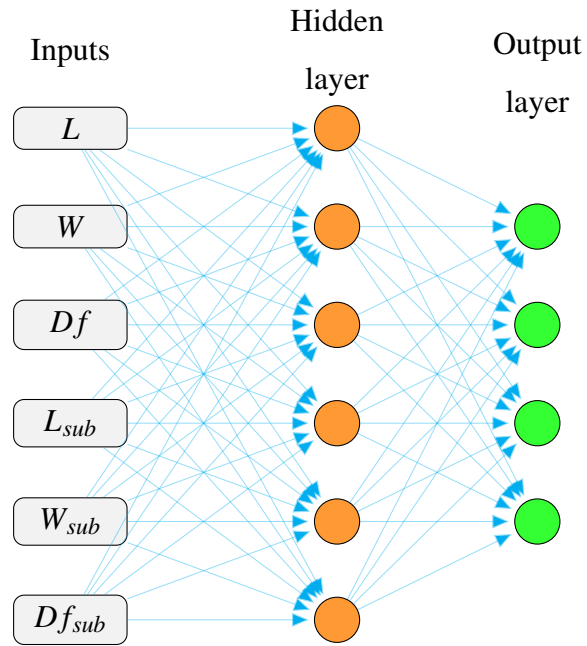


Figure 5.9 Diagram of artificial neural network

Softmax function is chosen for transfer function of it. Training method of the network is Levenberg-Marquardt algorithm (LMA). LMA was developed for finding minimum of a function which is defined as the sum of squares of nonlinear functions

(Marquardt, 1963; Lourakis, 2005). LMA was applied to this feedforward network as the same way that was represented in work of Hagan and Menhaj (Hagan & Menhaj, 1994). Performance function of network was set to mean squared error.

Levenberg-Marquardt backpropagation training is a combination of gradient descent and Gauss-Newton methods. It contains advantages of both methods. Gradient descent is a stable approach but it needs much time to converge. Update rule of basic gradient descent training method is:

$$w_{k+i} = w_k - \alpha g_k \quad (5.8)$$

where w_k is current weights, w_{k+i} is updated weights, α is learning rate and g_k is gradient. Updating continues until reaching to minimum of error. The calculation of the gradient is:

$$g_k = \frac{\partial E(\mathbf{x}, \mathbf{w})}{\partial \mathbf{w}} = \left[\frac{\partial E}{\partial w_1} + \frac{\partial E}{\partial w_2} + \dots + \frac{\partial E}{\partial w_n} \right]^T \quad (5.9)$$

where E is sum square error,

$$E(\mathbf{x}, \mathbf{w}) = \sum_{p=1}^P \sum_{n=1}^N \frac{1}{2} e_{p,m}^2 \quad (5.10)$$

$$e_{p,m} = d_{p,m} - o_{p,m} \quad (5.11)$$

d is desired output, o is actual output and e is training error.

The key point of gradient descent training method is selecting proper learning rate (α). Higher learning rates may not be converge to minima. On the other hand lower learning rates can take too much time to get results. Another disadvantage of lower learning rate is the risk of converging to a local minima. This situation may happen in some initial points.

Another approach, Gauss-Newton algorithm works according to the update rule:

$$w_{k+i} = w_k - (J_k^T J_k)^{-1} J_k e_k \quad (5.12)$$

J is Jacobian matrix of error function and e is training error. Gauss-Newton method is faster than Gradient descent. However it is successful if quadratic approximation of error function is reasonable. Otherwise it cannot converge.

Levenberg-Marquardt backpropagation training method blends two algorithm in one step. The updating rule of the method is:

$$w_{k+i} = w_k - (J_k^T J_k + \mu I)^{-1} J_k e_k \quad (5.13)$$

where μ is combination coefficient and must be positive. I is identity matrix. Updating rule is adjusted by increasing or decreasing μ . This results a stable and fast training process. Also the risk of convergence to a local minima is decreased dramatically.

5.2.3 Classification Results

According to our tests, classifier achieved 96.7% true detection rate. Confusion matrix of networks with all features (L , W , Df , L_{sub} , W_{sub} , Df_{sub}) and only main features (L , W , Df) are shown at Table 5.1, 5.2. As it was stated in Motion feature extraction section, addition of sub features improved performance of classifier.

Table 5.1 Confusion matrix of network with all features.

	G1	G2	G3	G4	Total
G1	25.0%	2.5%	0%	0%	90.9%
G2	0%	22.5%	0.8%	0%	96.4%
G3	0%	0%	24.2%	0%	100%
G4	0%	0%	0%	25.0%	100%
Total	100%	90%	96.7%	100%	96.7%

The most beneficial situation of adding sub-feature was classifying Group 2. It can be observed from Table 5.2 that classification error of Group 2 was the higher than other cases.

The main reason of this problem is that Group 2 covers all motions between straight and semi-complex. A detailed motion analysis is needed to separate this group from

Table 5.2 Confusion matrix of network without sub-features.

	G1	G2	G3	G4	Total
G1	23.4%	5.8%	0%	0%	80.0%
G2	0.8%	18.4%	1.8%	0%	88.0%
G3	0.8%	0.8%	23.3%	1.7%	87.5%
G4	0%	0%	0%	23.3%	100%
Total	93.3%	73.3%	93.3%	93.3%	88.3%

straight motion. Including sub-features into the artificial neural network added ability of detecting sort term complex movements to classifier. As a result, this homogeneity analysis decreased classification errors related with Group 2 successfully.

It was observed that linearity decreased from straight to complex while wobble and fractal dimensions increased. Moreover, correlations between motion groups and features can be analysed at figure 5.10. This figure shows that classification process was not dominated by a single feature.

Features of straight motion are consisted of higher L and lower W and Df . Slightly lower L or higher W or Df is resulted changing of the motion type into Curly motion. On the other hand, in semi-complex and complex motions L is very lower as expected. Difference between semi-complex and complex motions are determined by the values of W , Df and their sub-features.

Furthermore, performance addition of sub-features can be seen at Figure 5.10. For example, 14th window was labelled semi-complex, while 15th window was complex. These two windows have similar feature values of L , W . Also there is a slight change at Df . However there is a bigger difference of W_{sub} . That makes it the most distinctive feature in this case.

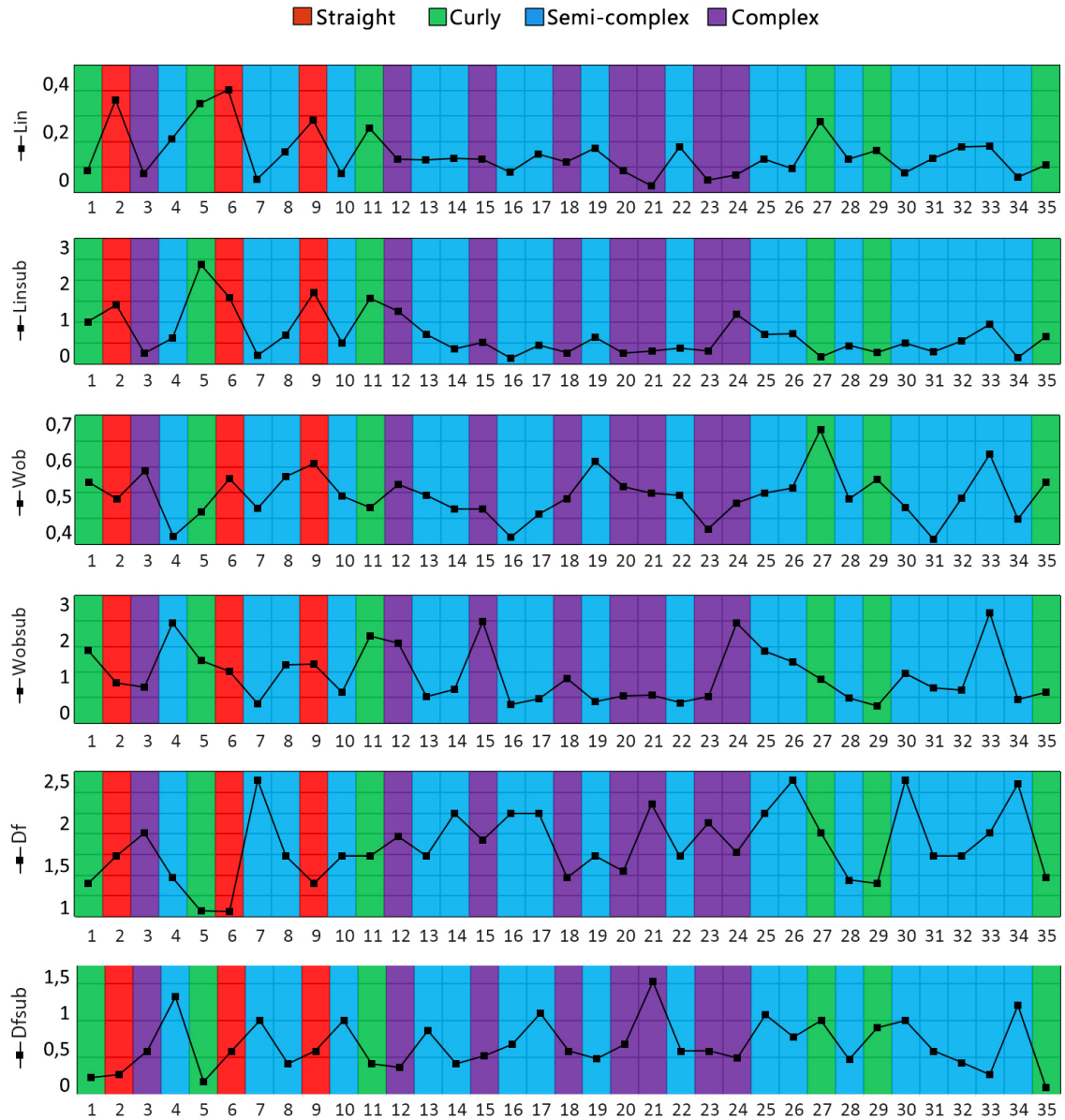


Figure 5.10 Relations between motion types and features for 35 tracking windows (140 seconds) of a sample.

CHAPTER SIX

RESULTS OF ECOTOXICITY ANALYSIS AND MOTION BEHAVIOR CLASSES

Artemia nauplii were examined under different concentration of potassium dichromate added into the mediums. Examinations were occurred by 20 different *Artemia salina* nauplii for each concentration and test group. Average percentage of motion types according to analyses are shown graphically at Figure 6.1 - 6.6. This figures show the average values of 20 different tests for each case.

It was clearly observed that toxic matter considerably effects motion behavior of *Artemia nauplii*. At the first moments of the experiments, the movements of nauplii were commonly formed by curvy and semi complex type. Also, about %15 straight motions determined at this stage. Percentage of the complex motions were found barely. On the other hand, following observations showed semi-complex and complex motion were increased. Moreover, last session of observations were dominated by complex motion. Effect of toxic matter in metabolism of nauplii reached to higher levels when the percentage of complex motion increased to %50 or more. This situation was called complex phase. After this stage, nauplii died a few hours later.

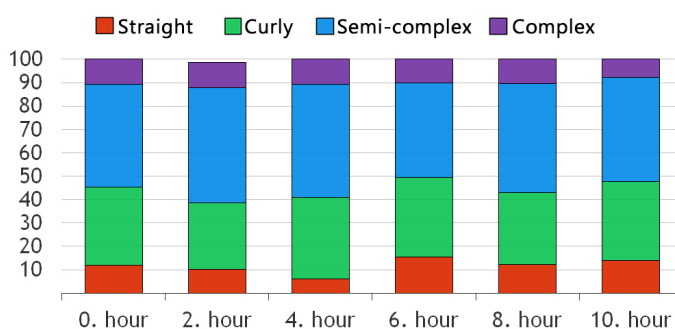


Figure 6.1 Motion analysis of all *Artemia nauplii* in control group.

In addition, Figure 6.1 presents that movements of *Artemia* in control. Same analysis procedure was performed on another set of animals which exposed to artificial seawater with no potassium dichromate. Motion characteristics of the control group did not show any significant change over time. Motions consisted of straight and semi-complex patterns. Complex type happened scarcely. This was the natural motion

behavior of *Artemia Salina*. Comparison of both test groups indicates that the reason of change in the swimming behavior of *Artemia salina* was due to toxic effect of potassium dichromate.

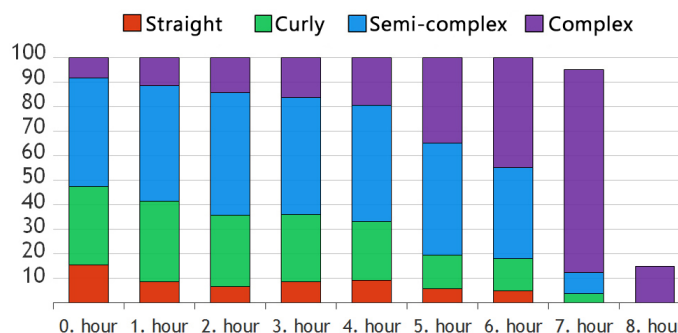


Figure 6.2 Motion analysis of all *Artemia* nauplii in 100 mg/L $K_2Cr_2O_7$ added solution.

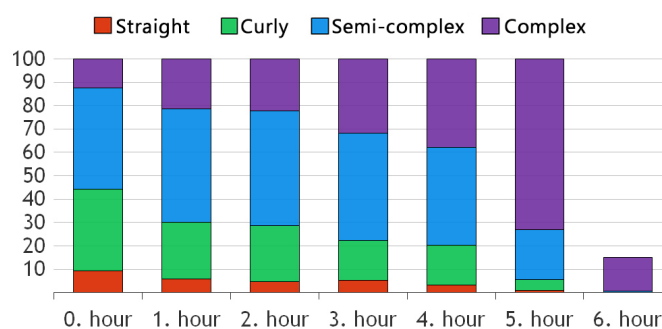


Figure 6.3 Motion analysis of all *Artemia* nauplii in 125 mg/L $K_2Cr_2O_7$ added solution.

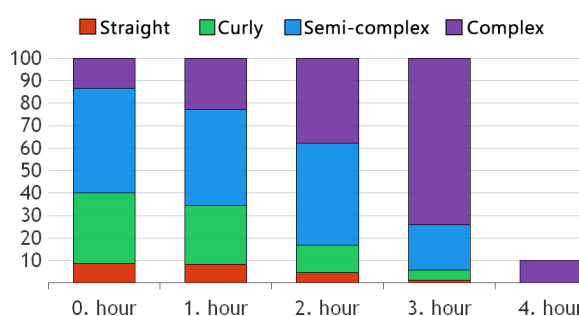


Figure 6.4 Motion analysis of all *Artemia* nauplii in 150 mg/L $K_2Cr_2O_7$ added solution.

Furthermore, impact speed of potassium dichromate is not similar in all cases. Higher concentrations cause sharper motion behavior alterations. The difference can be observed clearly at Figure 6.2 - 6.6. For example, motion types changed dramatically only in one hour at 200 mg/L experiments (Figure 6.6). However this transformation happened smoothly at 100 mg/L (Figure 6.2) and 125 mg/L case (Figure 6.3).

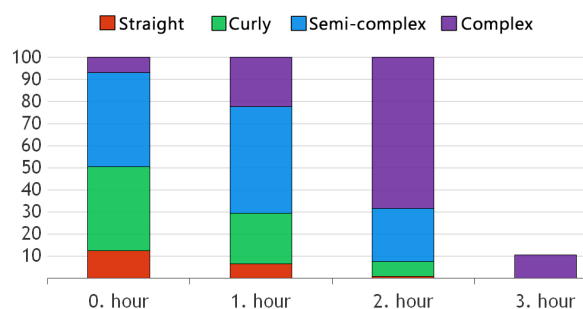


Figure 6.5 Motion analysis of all *Artemia* nauplii in 175 mg/L $K_2Cr_2O_7$ added solution.

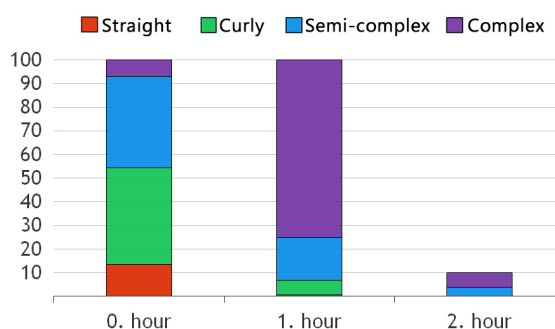


Figure 6.6 Motion analysis of all *Artemia* nauplii in 200 mg/L $K_2Cr_2O_7$ added solution.

Thereby, our study showed that motion analysis have to be evaluated with the time factor for detecting the concentration of toxic matter. Time of complex phase is the key element because the necessary time to reach complex phase was different for each concentrations of toxic matter (Figure 6.7).

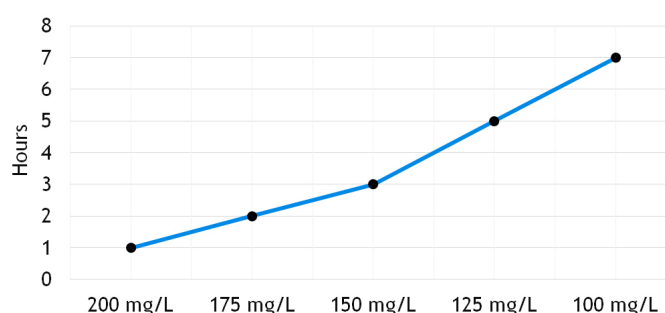


Figure 6.7 Necessary time to reach complex phase for different $K_2Cr_2O_7$ concentrations.

The main reason for this difference is the diffusion speed of the potassium dichromate from medium to the metabolism of nauplii. Higher concentrations of toxic matters interpenetrate to nauplii faster and cause sharper effects on motion types. That is why the time of the complex phase was used to determine the concentration of

potassium dichromate in an unknown medium.

Figure 6.8 shows the detailed motion analysis example of one nauplius under different conditions. These timeline charts are important to clarify the distribution of motion types. They show that the dominated motion types happened homogeneously during observation. This fact is supported by relatively low standard deviation value of dominated motion types (Table 6.1, 6.2). Moreover, it can be observed that transition between motion types happened sequentially in most situations.

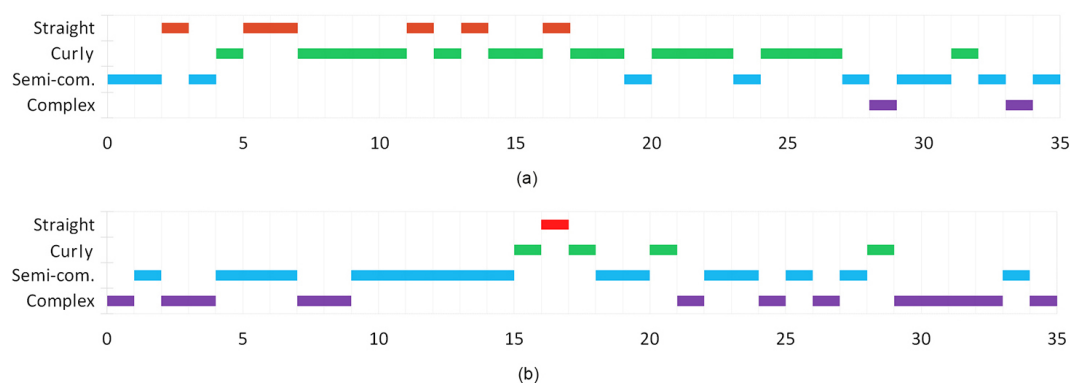


Figure 6.8 Timeline chart of motion analysis of one *Artemia* nauplius for 35 tracking windows (140 seconds); (a) control group at 3rd hour, (b) in 150 mg/L $K_2Cr_2O_7$ solution at 3rd hour.

Table 6.1 All results of control trials.

0. hour				2. hour			
G1	G2	G3	G4	G1	G2	G3	G4
12.03%	33.34%	43.87%	10.75%	10.06%	28.50%	49.30%	10.93%
±3.84	±6.098	±6.36	±4.52	±4.96	±8.33	±8.85	±4.69

4. hour				6. hour			
G1	G2	G3	G4	G1	G2	G3	G4
5.97%	34.82%	48.51%	10.69%	15.50%	33.86%	40.61%	10.02%
±4.55	±9.46	±8.76	±4.94	±5.14	±6.50	±8.01	±4.32

8. hour				10. hour			
G1	G2	G3	G4	G1	G2	G3	G4
12.09%	30.77%	46.62%	10.51%	13.87%	33.77%	44.69%	7.67%
±4.01	±6.76	±8.18	±3.78	±2.87	±5.47	±5.34	±2.17

Table 6.1 and 6.2 shows specific percentages of motion types for each trial. Barely seen motion types have higher standard deviation. In this case, these circumstances can be considered as a supplementary data for detecting dominated motion types.

Table 6.2 All results of toxic included trials.

	0. hour				1. hour				2. hour			
	G1	G2	G3	G4	G1	G2	G3	G4	G1	G2	G3	G4
100 mg/L	15.52% ±3.99	31.87% ±7.12	44.34% ±13.63	8.25% ±3.92	9.00% ±2.89	33.00% ±7.28	47.00% ±7.73	12% ±4.23	6.72% ±2.29	29.12% ±4.01	49.72% ±3.79	14.42% ±4.52
125 mg/L	9.48% ±2.67	34.79% ±13.49	43.28% ±7.24	12.43% ±3.717	6.00% ±2.27	24.00% ±14.88	48.00% ±6.27	22.00% ±4.41	4.82% ±2.7535	23.80% ±8.20	49.12% ±3.32	22.24% ±2.27
150 mg/L	8.63% ±7.45	31.49% ±5.89	46.52% ±5.78	13.33% ±3.98	8.00% ±3.42	26.00% ±6.83	43.00% ±5.06	23.00% ±5.18	4.59% ±2.81	12.27% ±5.44	45.34% ±7.89	37.78% ±8.78
175 mg/L	12.43% ±4.06	38.04% ±5.69	42.65% ±5.58	6.86% ±3.03	7.00% ±3.03	23.00% ±3.05	48.00% ±4.19	22.00% ±5.03	0.67% ±0.82	6.74% ±3.71	24.05% ±7.63	68.53% ±10.55
200 mg/L	13.56% ±3.20	40.67% ±7.40	38.78% ±7.52	6.96% ±3.09	1.00% ±0.84	6.00% ±4.16	18.00% ±7.11	75.00% ±8.85	-	-	-	-

	3. hour				4. hour				5. hour			
	G1	G2	G3	G4	G1	G2	G3	G4	G1	G2	G3	G4
100 mg/L	8.76% ±2.53	27.17% ±5.39	47.80% ±5.49	16.25% ±4.62	9.11% ±3.76	23.98% ±5.18	47.59% ±5.84	19.31% ±4.95	5.73% ±3.28	13.73% ±3.93	45.81% ±5.09	34.72% ±4.45
125 mg/L	5.25% ±2.97	17.06% ±8.75	45.90% ±6.02	31.78% ±2.88	3.40% ±2.48	17.01% ±10.93	41.67% ±6.612	37.92% ±7.95	0.89% ±0.93	4.75% ±5.21	21.27% ±7.01	73.08% ±8.65
150 mg/L	1.31% ±1.51	4.42% ±3.02	20.25% ±6.03	74.01% ±8.59	0% ±0	0% ±0	0% ±0	100% ±0	-	-	-	-
175 mg/L	-	-	-	-	-	-	-	-	-	-	-	-
200 mg/L	-	-	-	-	-	-	-	-	-	-	-	-

	6. hour				7. hour				8. hour			
	G1	G2	G3	G4	G1	G2	G3	G4	G1	G2	G3	G4
100 mg/L	5.03% ±3.44	12.95% ±4.51	37.08% ±5.63	44.93% ±10.39	0% ±0	2.94% ±2.44	9.20% ±6.48	86.93% ±7.47	0% ±0	0% ±0	0% ±0	100% ±0
125 mg/L	0% ±0	0% ±0	0% ±0	95.24% ±3.37	-	-	-	-	-	-	-	-
150 mg/L	-	-	-	-	-	-	-	-	-	-	-	-
175 mg/L	-	-	-	-	-	-	-	-	-	-	-	-
200 mg/L	-	-	-	-	-	-	-	-	-	-	-	-

CHAPTER SEVEN

CONCLUSION

This thesis presented the possibility to make a toxicity testing by taking advantage of *Artemia salina*'s motion behavior analysis. Motion behaviours of the organism were classified into four types. The effect of the toxic matter was determined by the changing of motion types.

Artemia salina nauplii were hatched under the same conditions. They were used at instar II-II stages which was the most toxic sensitive stage of nauplii. On the other hand, necessary chemical solutions were prepared. Five different concentration of potassium dichromate included solutions were used as medium of toxicity testing. The same testing procedure were also applied to a control group that were examined under non-toxic medium.

Movements of nauplii were recorded by the stereo recording system. It was used to identify the motion trajectory of *Artemia salina* nauplii. The system was not designed by sophisticated components but it was performed necessary success for application of the test. Basically, the set-up consists of two industrial GigE vision cameras, two lenses and a PC. Also a stereo recorder software was developed under Microsoft Visual C# Express to capture synchronised video pairs. After recording process, Matlab software was used for further process. Position of nauplii were detected in 2D coordinate systems for each video file. 3D Cartesian coordinates were calculated by obtained data from two stereo recorded video pairs. The next step was the extracting features from motion trajectories and classifying the motion types. Tests were repeated in four sessions for each concentrations of toxic matter and control group. Similar results of each session show that this test is time invariant. Finally average percentages of motion types was collected from toxicity testing trials in different concentration of toxic matter included medium. Analyses were performed by determining percentage of motion types (straight, curly, semi-complex, complex).

At the manual bioassay applications, results are evaluated by *death* or *not death* status. However, in our proposed system, there is no requirement to wait until the

death of nauplii because more detailed motion analysis can give meaningful results before death status. In addition, this system provides quantitative evolution without human caused errors.

Moreover, this test is considerably cheaper, easy accessible and flexible. The method of this work can be adapted for other type of toxic matters and organisms. The only essential and compelling part is the calibration of the system for the new kind of toxic and organism. Another property that can be adopted to this system in feature is real time process. Real time application can definitely decrease the concentration interval of toxic matter and can generate much more precise results.

REFERENCES

- AVT GigE Installation Manual* (2014). Retrieved 13 March 2014, from http://1stvision.com/cameras/AVT/dataman/GigE_Installation_Manual_V2.0.pdf.
- Alyuruk, H., Demir, G. K., & Cavas, L. (2013). A video tracking based improvement of acute toxicity test on *Artemia salina*. *Marine and Freshwater Behaviour and Physiology*, 46(4), 251–266.
- Barahona, M., & Sánchez-Fortún, S. (1999). Toxicity of carbamates to the brine shrimp *Artemia salina* and the effect of atropine, BW284c51, iso-OMPA and 2-PAM on carbaryl toxicity. *Environmental Pollution*, 104(3), 469–476.
- Bartolomé, M. C., & Sánchez-Fortún, S. (2005). Effects of selected biocides used in the disinfection of cooling towers on toxicity and bioaccumulation in *Artemia* larvae. *Environmental Toxicology and Chemistry / SETAC*, 24(12), 3137–42.
- Brine Shrimp* (2014). Retrieved 03 February 2014, from <http://www.britannica.com/EBchecked/topic/79674/brine-shrimp>.
- Choi, Y.-s., & Lee, S.-j. (2009). Three-dimensional volumetric measurement of red blood cell motion using digital holographic microscopy. *Applied Optics*, 48(16), 2983–2990.
- Dickle, M., & Burrough, P. A. (1988). Using fractal dimensions for characterizing tortuosity of animal trails. *Physiological Entomology*, 13(4), 393–398.
- Geyter, C. D., & Geyter, M. D. (1998). Diagnostic accuracy of computer-assisted sperm motion analysis. *Human Reproduction*, 13(9), 2512–2520.
- Ghanbari, A., Nock, V., Blaikie, R., Chen, X., Chase, J. G., & Wang, W. (2010). Automated vision-based force measurement of moving *C. elegans*. In *2010 IEEE International Conference on Automation Science and Engineering*, 198–203.
- Ghanbari, A., Nock, V., & Johari, S. (2012). A micropillar-based on-chip system for continuous force measurement of *C. elegans*. *Journal of Micromechanics and Microengineering*, 22(9), 95009.

- Hagan, M. T., & Menhaj, M. B. (1994). Training feedforward networks with the Marquardt algorithm. *IEEE transactions on neural networks / a publication of the IEEE Neural Networks Council*, 5(6), 989–93.
- How does Hawk-Eye work?* (2014). Retrieved 26 June 2014, from <http://www.hawkeyeinnovations.co.uk/page/sports-officiating/tennis>.
- Heath, H. (1924). The external development of certain phyllopods. *Journal of Morphology*, 38(4), 453–483.
- Held, M., Komaromy, A., & Fulga, F. (2009). Dynamic behaviour of microorganisms on microstructures. *Microelectronic Engineering*, 86(4-6), 1455–1458.
- Hernando, M. D., Ejerhoon, M., Fernández-Alba, A. R., & Chisti, Y. (2003). Combined toxicity effects of MTBE and pesticides measured with *Vibrio fischeri* and *Daphnia magna* bioassays. *Water Research*, 37(17), 4091–8.
- James, R. C., Roberts, S. M., & Williams, P. L. (2003). *General Principles of Toxicology*, 1–34. John Wiley and Sons, Inc.
- Jasko, D. J. (1990). *The application and use of objective analysis of sperm motion characteristics for the evaluation of fertility in the stallion*. Ph.D. Thesis, Cornell University.
- Kokkali, V., Katramados, I., & Newman, J. (2011). Monitoring the effect of metal ions on the mobility of *Artemia salina* nauplii. *Biosensors*, 1(2), 36–45.
- Koutsaftis, A., & Aoyama, I. (2007). Toxicity of four antifouling biocides and their mixtures on the brine shrimp *Artemia salina*. *The Science of the Total Environment*, 387(1-3), 166–74.
- Koutsaftis, A., & Aoyama, I. (2008). Toxicity of Diuron and copper pyriithione on the brine shrimp, *Artemia franciscana*: the effects of temperature and salinity. *Journal of Environmental Science and Health. Part A, Toxic/Hazardous Substances & Environmental Engineering*, 43(14), 1581–5.

- Kusk, K., & Nyholm, N. (1992). Toxic effects of chlorinated organic compounds and potassium dichromate on growth rate and photosynthesis of marine phytoplankton. *Chemosphere*, 25(6), 875–886.
- The brine shrimp life cycle* (2014). Retrieved 01 April 2014, from <http://learn.genetics.utah.edu/content/gsl/artemia/>.
- Lee, S., & Seo, K. (2011). Three-dimensional motion measurements of free-swimming microorganisms using digital holographic microscopy. *Measurement Science and Technology*, 22(6), 064004.
- Loader, C. (2004). Smoothing: Local regression techniques. *Papers / Humboldt-Universität Berlin, Center for Applied Statistics and Economics (CASE)*, (2004,12).
- Lourakis, M. (2005). A brief description of the Levenberg-Marquardt algorithm implemented by levmar. *Foundation for Research and Technology - Hellas*.
- Mann, C. J., Yu, L., & Kim, M. K. (2006). Movies of cellular and sub-cellular motion by digital holographic microscopy. *Biomedical Engineering Online*, 5, 21.
- Marquardt, D. W. (1963). An Algorithm for least-squares estimation of nonlinear parameters. *Journal of the Society for Industrial and Applied Mathematics*, 11(2), 431–441.
- McFarlane, N. J. B., & Schofield, C. P. (1995). Segmentation and tracking of piglets in images. *Machine Vision and Applications*, 8(3), 187–193.
- Mortimer, S. T., & Mortimer, D. (1990). Kinematics of Human Spermatozoa Incubated Under Capacitating Conditions. *Journal of Andrology*, 11(3), 195–203.
- Okamura, H. (2000). Fate and ecotoxicity of the new antifouling compound Irgarol 1051 in the aquatic environment. *Water Research*, 34(14), 3523–3530.
- Panagoula, B., Panayiota, M., & Iliopoulou-Georgudaki, J. (2002). Acute toxicity of TBT and IRGAROL in *Artemia salina*. *International Journal of Toxicology*, 21(3), 231–3.

- Ruebhart, D. R., Cock, I. E., & Shaw, G. R. (2008). Brine shrimp bioassay: Importance of correct taxonomic identification of artemia (anostraca) species. *Environmental Toxicology*, 23(4), 555–560.
- Sheng, J., Malkiel, E., & Katz, J. (2006). Digital holographic microscope for measuring three-dimensional particle distributions and motions. *Applied Optics*, 45(16), 3893–3901.
- Sorgeloos, P. (1978). The use of Artemia nauplii for toxicity tests - A critical analysis. *Ecotoxicology and Environmental Safety*, 2, 249–255.
- Sudo, S., Tsuyuki, K., & Honda, T. (2008). Swimming mechanics of dragonfly nymph and the application to robotics. *International Journal of Applied Electromagnetics and Mechanics*, 27, 163–175.
- Svensson, B., & Mathiasson, L. (2005). Artemia salina as test organism for assessment of acute toxicity of leachate water from landfills. *Environmental Monitoring and Assessment*, 102(1-3), 309–321.
- Tamron M118FM25 specifications* (2014). Retrieved 13 April 2014, from https://www.tamron.co.jp/en/data/cctv_fa/m118fm25.html.
- DFK 23G618 color camera* (2014a). Retrieved 10 April 2014, from http://archive.theimagingsource.com/en_US/p/c7374d74/.
- Technical details industrial cameras: 23 Series - trigger and I/O* (2014b). Retrieved 10 April 2014, from http://archive.theimagingsource.com/en_US/p/d5934e91/.
- Goal line technology* (2014). Retrieved 27 June 2014, from <http://visual.ly/goal-line-technology>.